Eur. Phys. J. C 22, 535–561 (2001)
Digital Object Identifier (DOI) 10.1007/s100520100792

THE EUROPEAN PHYSICAL JOURNAL C

Proposed Post-LEP benchmarks for supersymmetry

M. Battaglia[1], A. De Roeck[1], J. Ellis[1], F. Gianotti[1], K.T. Matchev[1], K.A. Olive[1,2], L. Pape[1], G. Wilson[3]

[1] CERN, 1211 Geneva, Switzerland
[2] Theoretical Physics Institute, School of Physics and Astronomy, University of Minnesota, Minneapolis, MN 55455, USA
[3] Department of of Physics and Astronomy, Schuster Laboratory, University of Manchester, Manchester, UK

Received: 28 June 2001 / Revised version: 12 September 2001 /
Published online: 23 November 2001 –

Abstract. We propose a new set of supersymmetric benchmark scenarios, taking into account the constraints from LEP, $b \to s\gamma$, $g_\mu - 2$ and cosmology. We work in the specific context of the constrained MSSM (CMSSM) with universal soft supersymetry-breaking masses and vanishing trilinear terms, assuming that R parity is conserved. We propose benchmark points that exemplify the different generic possibilities in this context, including focus-point models, points where coannihilation effects on the relic density are important, and points with rapid relic annihilation via direct-channel Higgs poles. We discuss the principal decays and signatures of the different classes of benchmark scenarios, and make initial estimates of the physics reaches of different accelerators, including the Tevatron collider, the LHC, and e^+e^- colliders in the sub- and multi-TeV ranges. We stress the complementarity of hadron and lepton colliders, with the latter favoured for non-strongly-interacting particles and precision measurements. We mention features that could usefully be included in future versions of supersymmetric event generators.

1 Introduction

The completion of the LEP experimental programme brings to an end an era of precise electroweak measurements and the search for new particles with masses $\lesssim$ 100 GeV. With the start of Run II of the Fermilab Tevatron collider, the advent of the LHC and perhaps a linear e^+e^- collider, the experimental exploration of the TeV energy scale is beginning in earnest.

The best-motivated scenario for new physics at the TeV energy scale is generally agreed to be supersymmetry. Theoretically, it is compellingly elegant, offers the possibility of unifying the fermionic matter particles with the bosonic force particles, is the only framework thought to be capable of connecting gravity with the other interactions, and appears essential for the consistency of string theory. However, none of these fundamental arguments offer clear advice as to the energy scale at which supersymmetric particles might appear.

The first such argument was provided by the hierarchy problem: if supersymmetric particles weigh less than of order 1 TeV, they may stabilize the electroweak scale $m_Z \ll m_P \sim 10^{19}$ GeV. The heavier the supersymmetric particles, the more the fine-tuning of the model parameters required to fix m_Z at its observed value. However, it is difficult to attach quantitative significance to any specific measure of the amount of this fine tuning.

LEP has provided no direct evidence for any physics beyond the Standard Model, but it has provided several indirect hints that supersymmetry may indeed lie around the corner. One such hint was provided by LEP's very accurate measurements of the gauge couplings, which are highly consistent with a supersymmetric Grand Unified theory (GUT) if the supersymmetric partners of the Standard Model particles weigh less than about 1 TeV [1], as suggested by the hierarchy problem [2]. Secondly, the precise electroweak data from LEP and elsewhere suggest that the Higgs boson is relatively light [3]:

$$m_H \; = \; 98^{+58}_{-38} \; \mathrm{GeV} \tag{1}$$

in good agreement with the prediction of the minimal supersymmetric extension of the Standard Model (MSSM), if the squarks weigh $\lesssim$ 1 TeV. Direct searches at LEP provided the lower limit $m_H > 113.5$ GeV (95% CL) [4]. In the final weeks of its run, LEP provided tentative evidence for a Higgs boson weighing $115.0^{+1.3}_{-0.9}$ GeV [4], perfectly consistent with the range (1) expected on the basis of the precise LEP electroweak measurements, as well as with the MSSM. Indeed, the effective potential of the Standard Model would be so sensitive to destabilization by radiative corrections if this tentative LEP evidence were to be confirmed, that some form of supersymmetry would probably be needed to stabilize our familiar electroweak vacuum [5].

A completely independent motivation for supersymmetry at the TeV scale is provided by the cold dark matter advocated by astrophysicists and cosmologists. If R parity is conserved, as we assume here, the lightest supersymmetric particle (LSP) is an ideal candidate to constitute the cold dark matter, if it weighs $\lesssim$ 1 TeV. We assume here that the LSP is the lightest neutralino χ [6]. The relic LSP

density increases with the masses of the supersymmetric particles, so the cosmological upper limit $\Omega_\chi h^2 \leq 0.3$ may, in principle be used to set an upper limit on the sparticle masses. However, in practice, one must be careful not to discard 'funnels' in the MSSM parameter space where heavier sparticles may be permitted.

Finally, we should add that the recent precise measurement of the anomalous magnetic moment of the muon, $g_\mu - 2$, which is in apparent disagreement with the Standard Model at the 2.6-σ level [7], has led to many speculations about new physics at the TeV scale. Prominent among these have been various supersymmetric interpretations of the possible discrepancy. These offer further encouragement that supersymmetry might be discovered at the LHC or before. However, caution advises us to await confirmation of the initial experimental value of $g_\mu - 2$ and to seek consensus on the calculation of hadronic contributions to $g_\mu - 2$ before jumping to any conclusions.

Nevertheless, the front-running nature of the supersymmetric candidacy for new physics beyond the Standard Model has motivated many studies of its experimental signatures at future colliders. In order to focus these discussions, and to provide standards of comparison for different analyses, experiments and accelerators, specific benchmark choices of supersymmetric parameters have often been proposed. For example, several years ago, several such benchmark scenarios were used to evaluate the capabilities of the LHC for detecting supersymmetry [8–10]. More recently, analogous benchmarks have been used in linear collider studies [11].

Unfortunately, time has overtaken some of these benchmark scenarios, whose parameters have by now been excluded by direct experimental searches for superymmetry and the Higgs boson at LEP, or because they predict unacceptable values of $g_\mu - 2$ or $b \to s\gamma$ decay, or because they predict unacceptable values of the relic LSP density $\Omega_\chi h^2$.

The purpose of this paper is to propose a new set of benchmark supersymmetric model parameters that are consistent with the experimental constraints, as well as cosmology. They may therefore provide helpful aids for understanding better the complementarity of different accelerators in the TeV energy range. We restrict our attention to a constrained version of the MSSM (CMSSM) which incorporates a minimal supergravity (mSUGRA)-inspired model of soft supersymmetry breaking. In the CMSSM, universal gaugino masses $m_{1/2}$, scalar masses m_0 (including those of the Higgs multiplets) and trilinear supersymmetry breaking parameters A_0 are input at the supersymmetric grand unification scale. In this framework, the Higgs mixing parameter μ can be derived (up to a sign) from the other MSSM parameters by imposing the electroweak vacuum conditions for any given value of $\tan\beta$. Thus, given the set of input parameters determined by $\{m_{1/2}, m_0, A_0, \tan\beta, sgn(\mu)\}$, the entire spectrum of sparticles can be derived. Here we will further restrict our attention to $A_0 = 0$, for simplicity. We do not consider benchmarks for models with gauge- [12], gaugino- [13] or anomaly-mediated [14] supersymmetry breaking, or for models with broken R parity. Studies of these and other models would be interesting complements to this work, and we comment on them in the last Section of this paper.

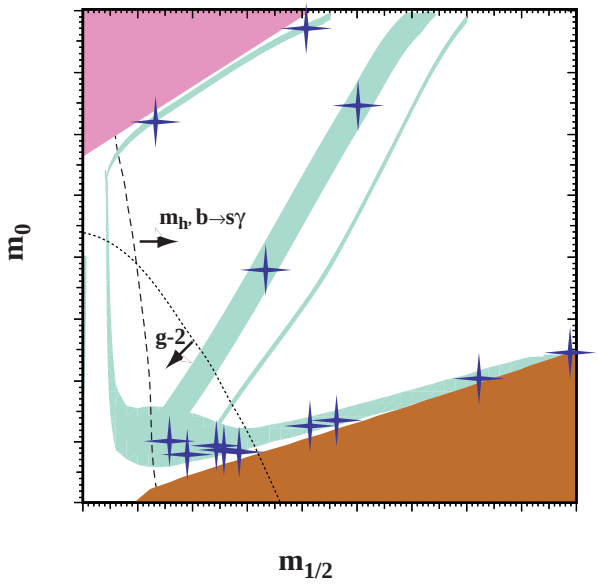

Fig. 1. Qualitative overview of the locations of our proposed benchmark points in a generic $(m_{1/2}, m_0)$ plane. The light (turquoise) shaded area is the cosmologically preferred region with $0.1 \leq \Omega_\chi h^2 \leq 0.3$, whose exact shape depends on the value of $\tan\beta$, and to some extent on the Standard Model inputs m_t, m_b and α_s. In the dark (brick red) shaded region at bottom right, the LSP is the charged $\tilde{\tau}_1$, so this region is excluded. Electroweak symmetry breaking is not possible in the dark (pink) shaded region at top left. The LEP experimental constraints, in particular that on m_h, and measurements of $b \to s\gamma$ exert pressure from the left side. The BNL E821 measurement of $g_\mu - 2$ favours relatively low values of m_0 and $m_{1/2}$ for $\mu > 0$. The CMSSM benchmark points we propose are indicated roughly by the (blue) crosses. We propose points in the 'bulk' region at bottom left, along the coannihilation 'tail' extending to larger $m_{1/2}$, in the 'focus-point' region at large m_0, and in the rapid-annilation 'funnel' that may appear at intermediate $m_0/m_{1/2}$ for large $\tan\beta$

Figure 1 illustrates qualitatively the CMSSM benchmark points we propose, superimposed on the regions of the $(m_{1/2}, m_0)$ plane favoured by LEP limits, particularly on m_h, $b \to s\gamma$ and cosmology. Electroweak symmetry breaking is not possible in the dark-shaded triangular region in the top left corner, and the lightest supersymmetric particle would be charged in the bottom right dark-shaded triangular region. The experimental constraints on m_h and $b \to s\gamma$ exert pressures from the left, as indicated, which depend on the value of $\tan\beta$ and the sign of μ. The indication of a deviation from the Standard Model in $g_\mu - 2$ disfavours $\mu < 0$ and large values of m_0 and $m_{1/2}$ for $\mu > 0$. The region where $\Omega_\chi h^2$ falls within the preferred range is indicated in light shading, its exact shape being dependent on the value of $\tan\beta$, and to some extent on the Standard Model inputs m_t, m_b and α_s. As discussed later in more detail, in addition to

the 'bulk' region at low m_0 and $m_{1/2}$, there is a coannihilation 'tail' extending to large $m_{1/2}$ [15,16], a 'focus-point' region at large m_0 near the boundary of the region with proper electroweak symmetry breaking [17], and narrow rapid-annilation 'funnels' at intermediate $m_0/m_{1/2}$ for large $\tan\beta$ [18–22]. The interplays of these features for different values of $\tan\beta, sgn(\mu)$, together with the corresponding proposed benchmark points, are shown in Figs. 2 and 3.

It is possible to learn much from general theoretical scans of the CMSSM parameter space, but the LHC experience also showed the complementary advantages of devoting some experimental attention to specific benchmark points [8], where the nitty-gritty problems of disentangling possible overlapping experimental signals and extracting measurements of CMSSM parameters can be confronted. We do not propose here a 'fair' statistical sampling of the allowed CMSSM parameter space. Rather, we propose benchmark points that span the essential range of theoretical possibilities, given our present knowledge. Some of the points we propose might soon become obsolete, for example because of Tevatron data or reductions in the error in $g_\mu - 2$. As seen in Fig. 1, many of the points we propose are spread over the allowed part of the 'bulk' region, at different values of $\tan\beta$. However, we also propose some points strung along the coannihilation 'tail', including one at the extreme tip, and two points each in the 'focus-point' region and the rapid-annihilation 'funnels'. Some of these points might appear disfavoured by fine-tuning arguments [23,24], but cannot be excluded. Taken together, the points we propose serve to highlight the different possible scenarios with which future colliders may be confronted. The input parameters for the benchmark points we propose, together with the resulting spectra as calculated using the code `SSARD` [25], are shown in Table 1.

The layout of this paper is as follows. In Sect. 2, we discuss the various experimental and other constraints on supersymmetric scenarios, and discuss how we implement them. Then, in Sect. 3, we introduce the set of benchmark scenarios we propose, motivating our choices in the multidimensional parameter space of the MSSM. For convenience, we introduce in Sect. 4 versions of these benchmarks calculated with suitable `ISASUGRA` [26] inputs, and we then use `ISASUGRA` to discuss the decay signatures of heavier sparticles, which are quite distinctive in some of these benchmark scenarios. Then, in Sect. 5 we take first looks at the physics reaches of various TeV-scale colliders, including the Tevatron, the LHC, a 500-GeV to 1-TeV linear e^+e^- collider such as TESLA, the NLC or the JLC, and a 3- to 5-TeV linear e^+e^- collider such as CLIC[1]. Finally, in Sect. 6, we review our results on the CMSSM benchmark scenarios we propose, discuss some of the future work that might be done to investigate further these benchmark supersymmetric scenarios and use them as a guide to understanding the physics opportunities offered by future colliders, and mention other possible scenarios that could also be studied.

[1] We comment in passing on the capabilities of $\mu^+\mu^-$ colliders

2 Experimental and cosmological constraints

We implement the experimental and cosmological constraints using a code `SSARD` that incorporates the two-loop running of the input soft supersymmetry-breaking parameters from the input scale $M_{\rm GUT}$ (defined as the scale where g_1 and g_2 meet) down to the electroweak scale, identified with m_Z. Exact gauge coupling unification is enforced, and the strong couplings constant $\alpha_s(m_Z)$ is a prediction. The μ parameter is extracted by minimizing the one-loop corrected effective potential [27,28] at the scale m_Z, while the pseudoscalar Higgs mass m_A is computed using the results of [29]. The radiative corrections to the light Higgs boson mass m_h are computed with the `FeynHiggs` code [30]. The full one-loop corrections to the physical chargino and neutralino masses are included [31–33]. The code also calculates $b \to s\gamma$ [34], $g_\mu - 2$ and the cosmological relic density using consistent conventions. We note, in particular, that the inclusion of one-loop corrections to chargino and neutralino masses is important for implementing accurately the LEP limits and the boundary of the region favoured by cosmology. We discuss later the problems encountered in matching the sparticle spectra obtained using this and other codes that implement these constraints using different approaches and/or approximations.

2.1 Sparticle searches

The most important direct experimental constraints on the MSSM parameter space are provided by LEP searches for sparticles [35] and Higgs bosons [4], the latter constraining the sparticle spectrum indirectly via radiative corrections, particularly those associated with third-generation supermultiplets. We use here the preliminary combined results that are based on data-taking at centre-of-mass energies up to about 208 GeV.

Upper limits at 95% CL on the the cross section for chargino-pair production were set [36] for all kinematically accessible chargino masses as a function of the neutralino mass, assuming that the branching ratio for $\chi^\pm \to W^\pm\chi^0$ was 100%. For neutralino masses approximately half the chargino mass, the upper limit obtained using 35 pb^{-1} of integrated luminosity at $\sqrt{s} > 207.5GeV$ is around 0.5 pb. These cross-section limits can be interpreted within the MSSM for some specific parameter values; for $\tan\beta = 2$, $\mu = -200$ GeV and sneutrino masses exceeding 300 GeV, the lower limit on the chargino mass is 103.5 GeV [36][2].

Similarly, the combined LEP data at $\sqrt{s}$ from 183 to 208 GeV were used to search for sleptons [37]. Events containing two charged leptons and missing energy were analysed and upper limits set on the cross section times branching-ratio squared for slepton-pair production followed by $\tilde{\ell} \to \ell + \chi$ decay, as functions of the slepton and neutralino masses. The limits vary substantially with

[2] There are also model-dependent limits on the supersymmetric parameter space derived from searches for associated $\chi\chi'$ production at LEP

Table 1. Proposed CMSSM benchmark points and mass spectra (in GeV), as calculated using `SSARD` [25] and `FeynHiggs` [30]. The renormalization-group equations are run down to the electroweak scale m_Z, where the one-loop corrected effective potential is computed and the CMSSM spectroscopy calculated, including the one loop corrections to the chargino and neutralino masses. The pseudoscalar Higgs mass m_A is computed as in [29]. Exact gauge coupling unification is enforced and the prediction for $\alpha_s(m_Z)$ is shown (in units of 0.001). It is also assumed that $A_0 = 0$ and $m_b(m_b)^{\overline{MS}} = 4.25$ GeV. For most of the points, $m_t = 175$ GeV is used, but for points E and F the lower value $m_t = 171$ GeV is used, for better consistency with [17]

Supersymmetric spectra

Model	A	B	C	D	E	F	G	H	I	J	K	L	M
$m_{1/2}$	600	250	400	525	300	1000	375	1500	350	750	1150	450	1900
m_0	140	100	90	125	1500	3450	120	419	180	300	1000	350	1500
$\tan\beta$	5	10	10	10	10	10	20	20	35	35	35	50	50
sign(μ)	+	+	+	−	+	+	+	+	+	+	−	+	+
$\alpha_s(m_Z)$	120	123	121	121	123	120	122	117	122	119	117	121	116
m_t	175	175	175	175	171	171	175	175	175	175	175	175	175
Masses													
$\lvert\mu(m_Z)\rvert$	739	332	501	633	239	522	468	1517	437	837	1185	537	1793
h^0	114	112	115	115	112	115	116	121	116	120	118	118	123
H^0	884	382	577	737	1509	3495	520	1794	449	876	1071	491	1732
A^0	883	381	576	736	1509	3495	520	1794	449	876	1071	491	1732
$H^\pm$	887	389	582	741	1511	3496	526	1796	457	880	1075	499	1734
χ_1^0	252	98	164	221	119	434	153	664	143	321	506	188	855
χ_2^0	482	182	310	425	199	546	291	1274	271	617	976	360	1648
χ_3^0	759	345	517	654	255	548	486	1585	462	890	1270	585	2032
χ_4^0	774	364	533	661	318	887	501	1595	476	900	1278	597	2036
$\chi_1^\pm$	482	181	310	425	194	537	291	1274	271	617	976	360	1648
$\chi_2^\pm$	774	365	533	663	318	888	502	1596	478	901	1279	598	2036
$\tilde{g}$	1299	582	893	1148	697	2108	843	3026	792	1593	2363	994	3768
e_L, μ_L	431	204	290	379	1514	3512	286	1077	302	587	1257	466	1949
e_R, μ_R	271	145	182	239	1505	3471	192	705	228	415	1091	392	1661
ν_e, ν_μ	424	188	279	371	1512	3511	275	1074	292	582	1255	459	1947
τ_1	269	137	175	233	1492	3443	166	664	159	334	951	242	1198
τ_2	431	208	292	380	1508	3498	292	1067	313	579	1206	447	1778
ν_τ	424	187	279	370	1506	3497	271	1062	280	561	1199	417	1772
u_L, c_L	1199	547	828	1061	1615	3906	787	2771	752	1486	2360	978	3703
u_R, c_R	1148	528	797	1019	1606	3864	757	2637	724	1422	2267	943	3544
d_L, s_L	1202	553	832	1064	1617	3906	791	2772	756	1488	2361	981	3704
d_R, s_R	1141	527	793	1014	1606	3858	754	2617	721	1413	2254	939	3521
t_1	893	392	612	804	1029	2574	582	2117	550	1122	1739	714	2742
t_2	1141	571	813	1010	1363	3326	771	2545	728	1363	2017	894	3196
b_1	1098	501	759	973	1354	3319	711	2522	656	1316	1960	821	3156
b_2	1141	528	792	1009	1594	3832	750	2580	708	1368	2026	887	3216

the masses, but typically the limits are 40 fb for the selectron and smuon search and 100 fb for the stau search. Within the context of the MSSM, these experimental limits lead to the exclusion of major portions of the right-handed slepton, neutralino mass plane at 95% CL. The mass limits were evaluated for $\tan\beta = 1.5$ and $\mu = -200$ GeV. For a neutralino mass of 40 GeV, the lower limits on the right handed slepton masses are 99.4 GeV, 96.4 GeV and 87.1 GeV for the selectron, smuon and stau respectively[3].

There are also important constraints on the squark and gluino masses from Run I of the Tevatron [38], extending up to 300 GeV if $m_{\tilde{q}} \sim m_{\tilde{g}}$, and additional constraints on stop and sbottom squarks from LEP. Since they do not play a rôle in our analysis, we do not discuss them in detail.

Analyses indicate that the experimental search results can be interpreted as chargino and slepton mass bounds close to the kinematic limits for most of the CMSSM pa-

[3] We note that, for both the chargino and the slepton searches, the sensitivity is much reduced for small values of the mass difference between the parent sparticle and the neutralino. However, this caveat is unimportant for the CMSSM as studied here

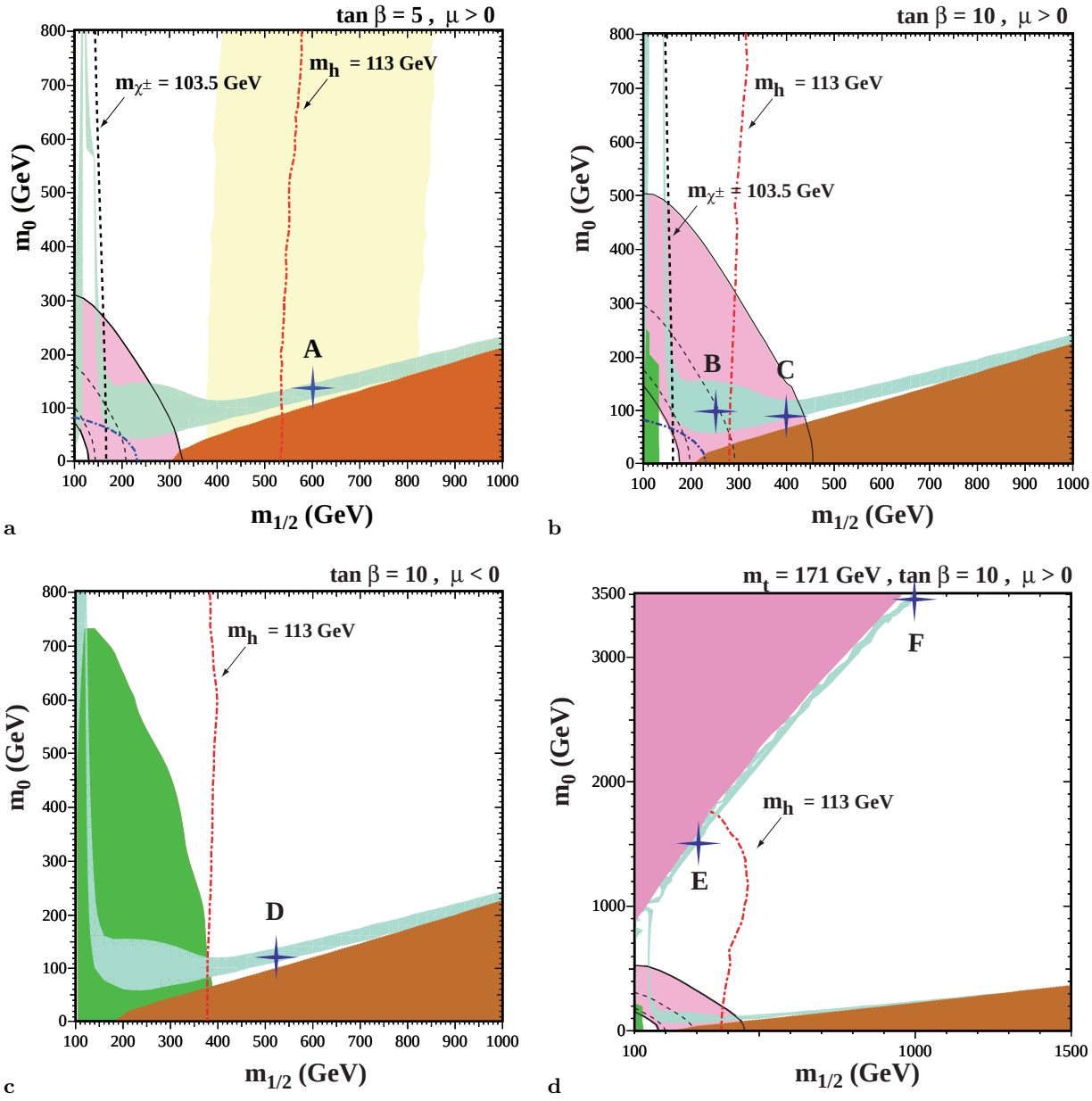

Fig. 2a–d. The $(m_{1/2}, m_0)$ planes for $\tan\beta =$ **a** 5 ($\mu > 0$), **b** 10 ($\mu > 0$), **c** 10 ($\mu < 0$), all for $m_t = 175$ GeV, and **d** 10 ($\mu > 0$) with $m_t = 171$ GeV. In each case we have assumed $A_0 = 0$ and $m_b(m_b)^{\overline{MS}}_{SM} = 4.25$ GeV, and used the `SSARD` code. The near-vertical (red) dot-dashed lines are the contours $m_h = 113$ GeV, as evaluated using the `FeynHiggs` code. In panel **a**, this is shown with a shaded band corresponding to a possible theoretical uncertainty of ± 2 GeV in m_h. The medium (dark green) shaded regions are excluded by $b \to s\gamma$. The light (turquoise) shaded areas are the cosmologically preferred regions with $0.1 \leq \Omega_\chi h^2 \leq 0.3$. In the dark (brick red) shaded regions, the LSP is the charged $\tilde{\tau}_1$, so this region is excluded. The regions allowed by the E821 measurement of a_μ at the 2-σ level are shaded (pink) and bounded by solid black lines, with dashed lines indicating the 1-σ ranges. Electroweak symmetry breaking is not possible in the dark (pink) shaded region at the top left of panel **d**. The (blue) crosses denote the proposed benchmark points A to F

rameter range [39]. Therefore, we show in panels (a,b) of Fig. 2 the contours (dot-dashed) in the $(m_{1/2}, m_0)$ plane corresponding to $m_{\chi^\pm} = 103.5$ GeV and $m_{\tilde{e}} = 99$ GeV. These contours are omitted from the remaining figures, for clarity.

As mentioned in the Introduction, the lower limit on the mass of a Standard Model Higgs boson imposed by the combined LEP experiments is 113.5 GeV [4]. This lower limit applies also to the MSSM for small $\tan\beta$, even if squark mixing is maximal. In the CMSSM, maximal mixing is not attained, and the $e^+e^- \to Z^0 + h$ production rate is very similar to that in the Standard Model, for all values of $\tan\beta$. Therefore, the LEP hint for a Higgs boson weighing $115.0^{+1.3}_{-0.9}$ GeV [4], which is compatible with the

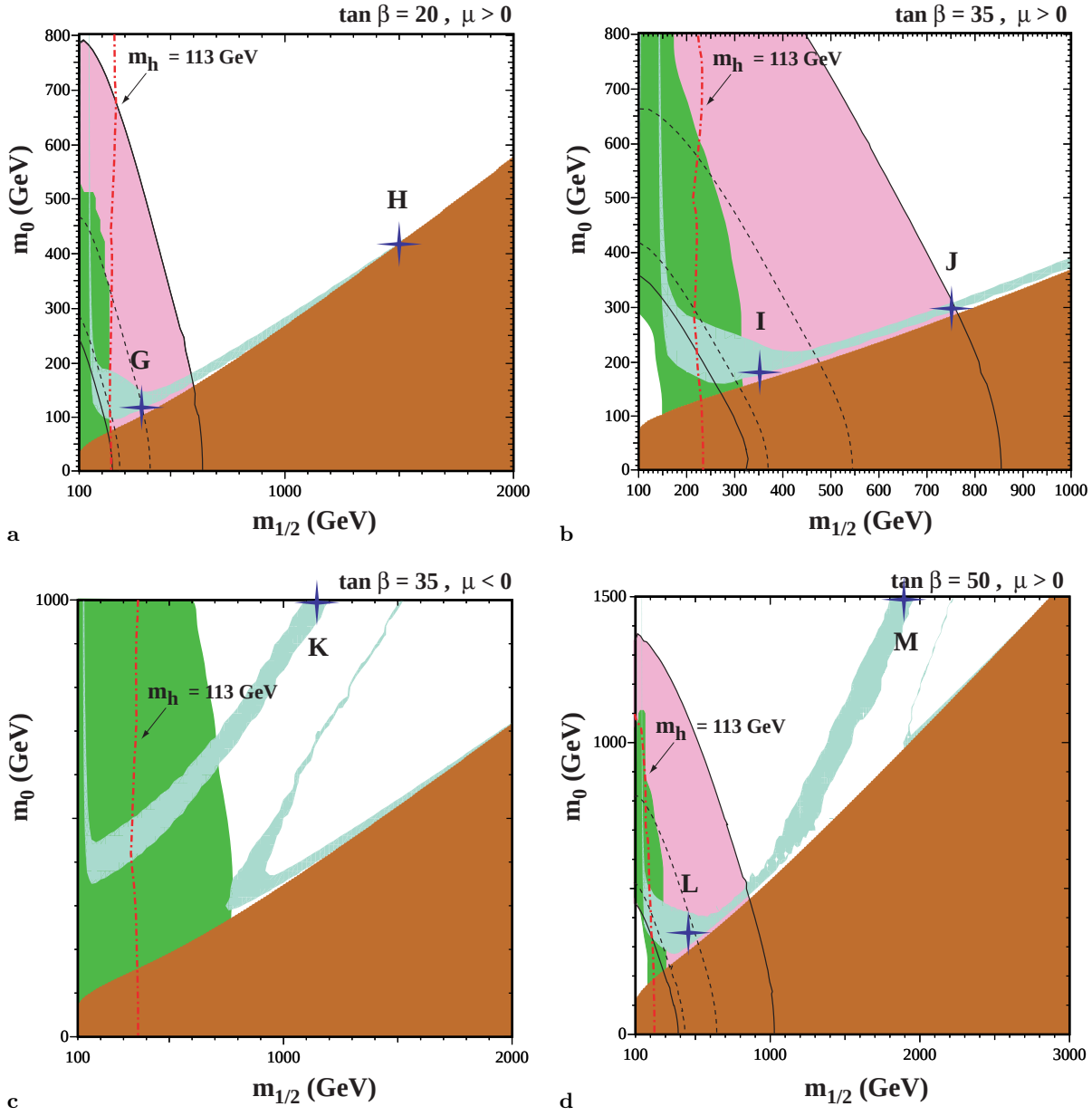

Fig. 3a–d. The $(m_{1/2}, m_0)$ planes for $\tan\beta =$ **a** 20 ($\mu > 0$), **b** 35 ($\mu > 0$), **c** 35 ($\mu < 0$), and **d** 50 ($\mu > 0$), found using SSARD and assuming $A_0 = 0, m_t = 175$ GeV and $m_b(m_b)^{\overline{MS}}_{SM} = 4.25$ GeV. The notations are the same as in Fig. 2. The (blue) crosses denote the proposed benchmark points G to M. At larger $\tan\beta$, the size as well as the exact shape of the cosmologically preferred region obtained is subject to considerable uncertainty, and different programs yield different answers for the same fixed values of the input parameters. The differences arise due to different calculational algorithms, and to neglecting different sets of higher-order terms. We elaborate more on these issues in Sect. 4

background-only hypothesis at the 0.4% CL, can also be interpreted in the CMSSM.

To calculate theoretically the mass of the lightest MSSM Higgs boson, we use the FeynHiggs code [30], which includes one-loop effects and also the leading two-loop contributions, and gives results that are somewhat higher than those obtained using [40]. In order to account for uncertainties in theoretical calculations of m_h in the MSSM [30] for any given value of m_t, we consider this LEP range [4] to be consistent with CMSSM parameter choices that yield 113 GeV $\leq m_h \leq$ 117 GeV. The theoretical value of m_h in the MSSM is quite sensitive to m_t, the pole mass of the top quark: we use $m_t = 175$ GeV as default, but mention explicitly the cases where $m_t = 171$ GeV has been used. Calculations of the Higgs mass and other quantities are also sensitive to the bottom-quark mass (particularly at large $\tan\beta$), for which we choose $m_b(m_b)^{\overline{MS}} = 4.25$ GeV for the running mass. All but one of the benchmark points we propose satisfy $m_h > 113$ GeV for $m_t = 175$ GeV. In view of the expected accuracy

$\sim$ 3 GeV of the `FeynHiggs` code, we therefore consider that all the proposed points are compatible with the LEP lower limit of 113.5 GeV [4].

2.2 $b \to s\gamma$ decay

We implement [34] the new NLO $b \to s\gamma$ calculations of [41] when $\tilde{M} > 500$ GeV, where $\tilde{M} = \mathrm{Min}(m_{\tilde{q}}, m_{\tilde{g}})$. Otherwise, we use only the LO calculations and assign a larger theoretical error. For the experimental value, we combine the CLEO measurement with the recent BELLE result [42], assuming full correlation between the experimental systematics[4], finding $\mathcal{B}(b \to s\gamma) = (3.21 \pm 0.44 \pm 0.26) \times 10^{-4}$. In our implementation, we allow CMSSM parameter choices that, after including the theoretical errors σ_{th} due to the scale and model dependences, may fall within the 95% confidence level range $2.33 \times 10^{-4} < \mathcal{B}(b \to s\gamma) < 4.15 \times 10^{-4}$. In general, we find in the regions excluded when $\mu < 0$ that the predicted value of $\mathcal{B}(b \to s\gamma)$ is larger than this measured range, whereas, when $\mu > 0$, the exclusion results from $\mathcal{B}(b \to s\gamma)$ being smaller than measured. Table 2 shows the values of $\mathcal{B}(b \to s\gamma)$ calculated in our proposed benchmark scenarios.

2.3 Muon anomalous magnetic moment

The BNL E821 experiment has recently reported [7] a new value for the anomalous magnetic moment of the muon: $g_\mu - 2 \equiv 2 \times a_\mu$, which yields an apparent discrepancy with the Standard Model prediction at the level of 2.6 σ:

$$\delta a_\mu \; = \; (43 \pm 16) \times 10^{-10}. \qquad (2)$$

The largest contribution to the stated error is due to statistics, and is expected to be reduced soon by a factor two or more. The systematic errors reported by the BNL E821 experiment are considerably smaller in magnitude. The largest uncertainty in the Standard Model prediction is that due to the hadronic contributions: $\delta a_\mu^{had} \sim 7\times10^{-10}$. The largest contribution to a_μ^{had} is in turn due to vacuum polarization diagrams, with the most important uncertainty being that in the low-energy region around the ρ^0 peak. The uncertainty in the hadronic vacuum polarization in this energy region may be reduced by combining the e^+e^- annihilation data with those from $\tau^\pm \to \rho^\pm\nu$ decay. There is also a hadronic contribution from light-by-light scattering diagrams, which has been estimated using chiral perturbation theory, and is thought to yield a smaller uncertainty in a_μ^{had} [43].

The estimate of the hadronic vacuum-polarization contributions [44] used in the E821 paper [7] does not include the latest e^+e^- data from Novosibirsk [45] and Beijing [46], nor the most recent τ decay data from CLEO [47][5]. However, these are thought unlikely [48] to change the overall picture: we recall that the quoted hadronic error $\sim 7\times10^{-10}$ is much smaller than the apparent discrepancy and the experimental error. Advocates of new physics beyond the Standard Model may therefore be encouraged. However, a final conclusion must await the publication of more $g_\mu - 2$ data and the achievement of consensus on the hadronic contribution.

A priori, the BNL measurement favours new physics at the TeV scale, and we consider the best motivated candidate to be supersymmetry. Even before the hierarchy motivation for supersymmetry emerged, the potential interest of a_μ was mentioned, and a pilot calculation performed [49], followed by many others [50,51]. Some time ago, it was emphasized [51] that the BNL experiment would be sensitive to a large range of the parameter space of the CMSSM with universal soft superymmetry-breaking parameters at the input GUT scale, determining in particular the sign of the Higgs mixing parameter μ [51]. A large number of theoretical papers have discussed the interpretation of the BNL measurement within supersymmetry [52,53]. These calculations generally agree that $\mu > 0$ is favoured by the BNL measurement. The calculations we use in this paper are taken from [53], which are based on [54][6], including also the leading two-loop electroweak correction factor [56].

In this paper, we do not impose the BNL $g_\mu - 2$ constraint in the form (2), though we do bear it in mind in the selection of points, for example in the relative weighting of points with $\mu > 0$ and $\mu < 0$. About half of the points we propose yield values of δa_μ that are compatible with (2) within two standard deviations, and several of the points lie within one standard deviation. Table 2 shows the values of δa_μ calculated in our proposed benchmark scenarios.

2.4 Cosmological relic density

Like most analyses of CMSSM phenomenology for future colliders, we assume that R parity is conserved. This implies that the lightest supersymmetric particle (LSP) is stable, and hence should be present in the Universe today as a cosmological relic from the Big Bang, constituting part of the dark matter. If the LSP had either strong or electromagnetic interactions, it would bind with conventional matter to form anomalous heavy isotopes. These are not seen down to levels far below the calculated relic density, so the LSP can have only weak and gravitational interactions [6]. There are scenarios in which the LSP is not the supersymmetric partner of any of the Standard Model particles. For example, it might be the gravitino or axino. In these cases, cosmological constraints on the dark matter density cannot be used to constrain the CMSSM in a useful way, and values of $m_{1/2}$ and m_0 larger than those we discuss would also be allowed.

Among the supersymmetric partners of Standard Model particles, LEP data and direct searches for the scattering of cold dark matter particles appear to exclude the

[4] This is conservative, but the available information does not justify a less conservative approach, and this assumption is in any case not very important

[5] More data on τ decays can be expected from the LEP experiments and the B factories

[6] For other recent calculations, see [55]

Table 2. Derived quantities in the benchmark models proposed. In addition to the relic density $\Omega_\chi h^2$, the supersymmetric contribution to $a_\mu \equiv (g_\mu - 2)/2$ in units of 10^{-10}, and the $b \to s\gamma$ decay branching ratio 10^{-4}, we also display the amount of electroweak fine-tuning Δ^Ω (all of the above quantities are calculated using `SSARD`), and the amount of electroweak fine-tuning, calculated with the `BMPZ` code [33], using the `ISASUGRA 7.51` versions of the input parameters

Properties of proposed benchmark models

Model	A	B	C	D	E	F	G	H	I	J	K	L	M
$\Omega_\chi h^2$	0.26	0.18	0.14	0.19	0.31	0.17	0.16	0.29	0.16	0.20	0.19	0.21	0.17
δa_μ	2.8	28	13	-7.4	1.7	0.29	27	1.7	45	11	-3.3	31	2.1
$B_{s\gamma}$	3.54	2.80	3.48	4.07	3.40	3.32	3.10	3.28	2.55	3.21	3.78	2.71	3.24
σ_{th}	0.15	0.12	0.14	0.17	0.14	0.14	0.13	0.14	0.11	0.14	0.16	0.12	0.14
Δ	275	43	108	166	46	325	90	1056	76	272	477	128	1199
$(+\ \lambda_t)$	(292)	(47)	(117)	(177)	(153)	(559)	(97)	(1098)	(83)	(294)	(537)	(138)	(1276)
Δ^Ω	6.0	1.3	5.7	7.0	106	85	9.3	36	12	32	91	7.3	33
$(+\ \lambda_t)$	(6.0)	(1.3)	(5.9)	(7.0)	(372)	(1089)	(11)	(36)	(13)	(33)	(125)	(29)	(206)

possibility that the LSP is a sneutrino $\tilde{\nu}$ in the MSSM [57]. The most viable LSP candidate seems to be the lightest neutralino χ, and this is the hypothesis adopted here. Since the sparticle spectrum is explicitly calculable in the CMSSM, we concentrate on regions of its parameter space in which the LSP is a neutralino, to the exclusion of other regions.

Astrophysics and cosmology provide many independent arguments that most of the gravitating matter in the Universe is invisible. Some of this is certainly baryonic, but the consistency of cosmological nucleosynthesis calculations with the observed light element abundances suggest that most of the dark matter is non-baryonic [58]. This conclusion has been reinforced by recent estimates of the cosmological baryon density Ω_b based on microwave background data, which suggest [59]

$$\Omega_b h^2 \ \sim \ 0.02, \tag{3}$$

with an error of about 20%, where h is the present Hubble expansion rate in units of 100 km/s/Mpc. The Hubble Key Project [60] and other measurements indicate that $h^2 \sim 0.5$, again with an error of about 20%. The estimate (3) is much smaller than the corresponding estimate of the overall matter density [59]:

$$\Omega_m h^2 \ \sim \ 0.14 \pm 0.04. \tag{4}$$

We conclude that most of the matter in the Universe is in the form of non-baryonic dark matter, and hypothesize in this paper that it consists mainly of the lightest neutralino χ.

For the purpose of this paper, we assume

$$0.1 \ \leq \ \Omega_\chi h^2 \ \leq \ 0.3. \tag{5}$$

The upper limit being a conservative upper bound based only on the lower limit to the age of the Universe of 12 Gyr. Larger values of $\Omega_\chi h^2$ would require values of $m_{1/2}$ and m_0 larger than those we discuss, in general. Smaller values of $\Omega_\chi h^2$, corresponding to smaller values of $m_{1/2}$ and m_0, are certainly possible, since it is quite possible that some of the cold dark matter might not consist of LSPs. Axions and ultraheavy metastable relic particles are other candidates that might contribute. However, allowing smaller values of $\Omega_\chi h^2$ would open up only a very small extra area of the $(m_{1/2}, m_0)$ plane, as we see shortly.

We base our relic density calculations on a recent analysis [22] using `SSARD` that extends previous results [61] to larger $\tan\beta > 20$. We note here two important effects on the calculation of $\Omega_\chi h^2$ that were discussed in [22], which are due to improvements of previous calculations of $\chi - \tilde{\ell}$ coannihilations and direct-channel $\chi\chi$ annihilations through the heavier neutral MSSM Higgs bosons H and A [18–22]. Both of these effects extend the region of CMSSM parameter space consistent with cosmology out to values of m_0 and $m_{1/2}$ that were larger than those found at smaller values of $\tan\beta$ [15,61][7]. As we discuss later, good overall consistency was found [53] between these relic density calculations, the LEP and other sparticle mass limits, the LEP Higgs 'signal' and measurements of $b \to s\gamma$, and also the recent BNL measurement of $g_\mu - 2$ if $\mu > 0$. There is also a region of the $(m_{1/2}, m_0)$ plane at relatively large values of m_0, close to the higgsino LSP area, termed the 'focus-point' region. This is consistent with $b \to s\gamma$ for any $\tan\beta$, and may also be consistent with $g_\mu - 2$ if $\tan\beta$ is large and $m_{1/2}$ is relatively small, according to the `BMPZ` code [33] although not according to `SSARD` for the input parameter values used in Fig. 3d (see the discussion in Sect. 4).

Table 2 shows the values of $\Omega_\chi h^2$ calculated in our proposed benchmark scenarios.

2.5 Electroweak and cosmological fine-tuning

Here we discuss two distinct issues: the fine-tuning of CMSSM parameters that is required to obtain the electroweak scale, and the sensitivity of the cosmological relic density to input parameters.

[7] We note that the effect of relaxing the assumption of scalar-mass universality for the Higgs multiplets is generally to extend the allowed cosmological domain to larger $m_{1/2}$ and m_0 [39]

As mentioned in the Introduction, the TeV mass scale for supersymmetry is largely motivated by the gauge hierarchy problem: how to make the small electroweak scale $m_Z \ll m_P \sim 10^{19}$ GeV 'natural', without the need to fine-tune parameters at each order in perturbation theory [2]. This is possible if the supersymmetric partners of the Standard Model particles weigh $\lesssim 1$ TeV, but the amount of fine-tuning of supersymmetric parameters required to obtain the electroweak scale increases rapidly for sparticle masses $\gg 1$ TeV. In an attempt to quantify this, it was proposed [23] to consider the logarithmic sensitivities of the electroweak scale to the supersymmetric model parameters a_i:

$$\Delta \equiv \sqrt{\Sigma_i (\Delta_i)^2} : \Delta_i \equiv \frac{a_i}{m_Z} \frac{\partial m_Z}{\partial a_i}. \quad (6)$$

In the CMSSM with universal soft supersymmetry-breaking parameters, the fundamental parameters a_i include the common scalar mass m_0, the common gaugino mass $m_{1/2}$, the common trilinear parameter A_0 at the GUT scale, the supersymmetric Higgs mass parameter μ at the GUT scale and the supersymmetry-breaking Higgs mass parameter B at the GUT scale. These are the fundamental dimensionful parameters which are expected to be directly related to the physics responsible for breaking the electroweak symmetry and generating the correct size for the electroweak scale. In view of the sensitivity of the electroweak scale to the top (and possibly the bottom) Yukawa coupling $\lambda_t(\lambda_b)$, some (but not all) of the Yukawa couplings at the GUT scale are sometimes included among the fundamental parameters in (6)[8]. In what follows, we quote the values of Δ for both cases: first, considering the fine tuning only with respect to the dimensionful CMSSM parameters, and then including also the sensitivity to λ_t.

An analogous measure of the amount of fine-tuning needed to obtain in the CMSSM a relic density $\Omega_\chi h^2$ in the range preferred by cosmology has been proposed recently [24]:

$$\Delta^\Omega \equiv \sqrt{\Sigma_i (\Delta_i^\Omega)^2} : \Delta_i^\Omega \equiv \frac{a_i}{\Omega_\chi} \frac{\partial \Omega_\chi}{\partial a_i}. \quad (7)$$

In this case, we hold m_Z fixed, and therefore, the set of input parameters $\{a_i\}$ becomes $\{m_0, m_{1/2}, A_0, \tan\beta, sgn(\mu)\}$. The relic density is also quite sensitive to the values of the Standard Model parameters m_t and m_b.

Table 2 shows the values of Δ and Δ^Ω calculated in our proposed benchmark scenarios. The first (second) row for Δ shows the electroweak fine-tuning without (with) λ_t included among the a_i (the λ_b dependence of Δ is relatively mild). The first (second) row for Δ^Ω shows the cosmological fine-tuning without (with) m_t and m_b included among the a_i. The dependence of Δ^Ω on m_b is significant at high $\tan\beta$, particularly for point K, L and M. We see from Table 2 that, as a rule, the electroweak fine-tuning roughly scales with $m_{1/2}$ and is independent of m_0, if only the sensitivity to the dimensionful parameters is considered – this is in essence the focus-point phenomenon [63,64]. On the other hand, Δ^Ω behaves similarly to Δ, except in the 'focus-point' and rapid-annihilation 'funnel' regions, where it is found that there is a strong sensitivity of Ωh^2 to the input parameters [24].

We emphasize that fine tuning should not be confused with instability: the fact that CMSSM model parameters might need to be adjusted carefully in some cases does not mean that the resulting points in parameter space are inherently unstable. They are perfectly good electroweak vacua, and cannot be excluded *a priori*. The extent to which one cares about the amount of fine tuning depends on the underlying measure in CMSSM parameter space, which is of course unknown at present. Moreover, there are surely correlations between the input parameters, and it is known that these may reduce radically the apparent amounts of fine tuning. Finally, extending the spirit of (6) and (7), one might define alternative (or additional) measures of fine-tuning reflecting the sensitivities of other physical observables to the fundamental parameters, which might change again the relative weights of the points. For example, one could consider large CP-violating phases [65] and ask about the degree of fine-tuning required to bring various electric dipole moments in accord with experiment. One would then find that in this sense the bulk points are much more fine-tuned than the focus points [62], coannihilation 'tail' points [15] and rapid-annihilation 'funnel' points [22]. For these reasons, measures of fine tuning come with impressive health warnings on the packet. Hence, we do not use their values as selection criteria for benchmarks. However, we do see clearly that some models are more finely tuned than others. The values of Δ vary by a factor of 28 between benchmarks B and M (27 if λ_t is included among the a_i.), whereas the values of Δ^Ω vary over a factor 81 between benchmarks B and E (840 between benchmarks B and F if m_t is included among the a_i).

2.6 Combination of constraints

The interplays of all these constraints in the $(m_{1/2}, m_0)$ planes for some values of $\tan\beta$ are illustrated in Fig. 2 and 3. The very dark (red) triangular regions at large $m_{1/2}$ correspond to $m_{\tilde{\tau}_1} < m_\chi$, where $\tilde{\tau}_1$ is the lighter $\tilde{\tau}$ mass eigenstate. These regions are ruled out by the requirement that the LSP be neutral. We show as (red) dash-dotted lines the $m_h = 113$ GeV contour calculated using `FeynHiggs` [30]. We see that the Higgs mass bound from LEP excludes regions of small $m_{1/2}$, and has strongest impact at low $\tan\beta$.

The position of the Higgs constraint is very sensitive to the chosen mass contour at low $\tan\beta$, which is subject to theoretical uncertainties. To exemplify this sensitivity, we show in panel (a) of Fig. 2 a band around the 113 GeV Higgs mass contour corresponding to a potential theoretical uncertainty of $\pm$ 2 GeV. The thickness $\sim$ 450 GeV of the band is clearly significant for $\tan\beta = 5$. However, for larger $\tan\beta$, as the Higgs constraint moves to the left in $m_{1/2}$, the thickness of the ± 2 GeV band becomes significantly thinner. For clarity, it is not displayed in the

[8] For an extensive discussion of the philosophy behind these choices, see [62]

remaining panels of Fig. 2 and Fig. 3. However, we record that for $\tan\beta = 10, 20$ and $\mu > 0$, it is 100 - 200 GeV thick, increasing to 200 - 300 GeV thick for $\mu < 0$. At higher values of $\tan\beta \sim 50$, the band corresponding to the 111 - 115 GeV Higgs mass range is even thinner, $\sim 100 GeV$.

In a previous analysis, it was shown in [66] that the whole of the plane which is of cosmological interest is excluded by the Higgs bound for values of $\tan\beta \lesssim 3.5$. Hence, for the benchmarks, only values of $\tan\beta \geq 5$ were considered. The (dashed) bound on the chargino mass from LEP excludes very low $m_{1/2}$ values, almost independently of $\tan\beta$, and the LEP selectron constraint (dot-dashed) excludes a region around the origin in the ($m_{1/2}$, m_0) plane. We do not show them on all the panels in Figs. 2 and 3, but only in panels (a,b) of Fig.2 for $\tan\beta = 5, 10$ and $\mu > 0$: their locations are similar for the other CMSSM cases studied. The branching ratio for $b \to s\gamma$ excludes a dark (green) shaded area at low $m_{1/2}$. Its impact increases with increasing $\tan\beta$, and is larger for $\mu < 0$.

The cosmological constraint $0.1 \leq \Omega_\chi h^2 \leq 0.3$ allows a region shown in light grey (turquoise), which exhibits a narrowing coannihilation strip that extends at large $m_{1/2}$ into the domain where the $\tilde{\tau}_1$ is the LSP. This defines upper bounds on the allowed values of $m_{1/2}$ (and hence m_χ) in the coannihilation region, which are

$$m_{1/2} \sim 1400 \text{ GeV}, \; m_\chi \sim 600 \text{ GeV}, \qquad (8)$$

for $\tan\beta \lesssim 20$, increasing at larger $\tan\beta$: $m_{1/2} \lesssim 1900$ (2200) GeV is allowed for $\tan\beta = 35(50)$, as seen in (b, c, d) of Fig. 3. The 'tails' of these regions are potentially beyond the physics reach of the LHC, but are disfavoured by $g_\mu - 2$.

We also see in panels (c, d) of Fig. 3 the possibility of a 'funnel' extending to large $m_{1/2}$ and m_0 where an acceptable relic density is made possible by rapid direct-channel annihilation $\chi\chi \to H, A$. There is also an allowed cosmological strip at large m_0 where the LSP has a significant higgsino component, and as a result, neutralino annihilation to gauge boson pairs, as well as s-channel Higgs exchange are enhanced [17,67]. This region lies in the 'focus-point' region and is present in all panels with $\tan\beta > 5$, although for improved readability of the figures we choose to show it only in panel (d) in Fig. 2. Just above the focus-point region there is a shaded area with no acceptable electroweak symmetry-breaking solutions, and a light higgsino-like chargino near its boundary. Areas in Fig. 2 and 3 between the 'focus-point' and the other shaded cosmological regions have values of $\Omega_\chi h^2$ that are too large, and hence are excluded by the cosmological relic density constraint. As already commented, the unshaded areas at lower m_0 values have $\Omega_\chi h^2 < 0.1$, and hence are in principle allowed by cosmology[9]. However, the remaining parts of these regions compatible with other constraints are quite small[10].

Finally, we note that the $g_\mu - 2$ result prefers the diagonal band at low m_0 and $m_{1/2}$ shown in darker grey (pink). The one-sigma band is indicated by dashed lines and the full lines represent the two-sigma band. We see that there is good overall compatibility between $g_\mu - 2$ and the other constraints for $\tan\beta \gtrsim 10$ and $\mu > 0$. The $g_\mu - 2$ constraint disfavours large values of $m_{1/2}$ and m_0, excluding, for example, the tails of the cosmological region.

3 Proposed benchmark points

Supersymmetric benchmark points have a venerable history in physics studies for future colliders [9,11,68,69]. They were useful in showing how many spectroscopic measurements might be possible at the LHC, and in demonstrating the precisions possible there and with an e^+e^- linear collider. However, only about 3 out of the 26 points previously studied are clearly compatible with all the LEP constraints, though some cases may survive if the theoretical errors in calculating m_h are favourable to them. The points used previously also could not take into account the recent constraints from $b \to s\gamma$ and $g_\mu - 2$. Furthermore, many of the previous points also give unacceptably large relic densities. For instance, six points in CMSSM parameter space were studied in detail for the LHC [8]. None of them have survived the most recent LEP2 limits, dark matter constraints and $g_\mu - 2$ constraints.

We have chosen our proposed new benchmark points for $\tan\beta = 5$, 10, 20, 35 and 50 to span the possibilities in the preferred regions. The locations of the points in the $(m_{1/2}, m_0)$ planes for different values of $\tan\beta$ are shown in Figs. 2 and 3. As already remarked, the points are probably all consistent with the LEP Higgs mass constraint $m_h \geq 113.5$ GeV, once theoretical uncertainties are taken into account. We also took note of the $g_\mu - 2$ measurement, so that most points have $\mu > 0$ and several are within the 2-σ experimental range. In some cases, points with different values of $\tan\beta$ give rise to very similar particle spectra and decay characteristics, and it was decided to keep only one example, so as to avoid duplication. For this and many other reasons, the chosen points should not be considered an unbiased statistical sampling of the CMSSM possibilities. However, we did make an effort to probe the different possibilities. Thus, we include two 'focus-point' models, two in the coannihilation tails at large $m_{1/2}$, and two in rapid $\chi\chi \to H, A$ annihilation funnels, and we kept two points with $\mu < 0$.

The input parameters of the benchmark points, labelled from A to M, are listed in Table 1.

We now make some comments on the individual points.

A: The only allowed points for this small $\tan\beta = 5$ are far into the coannihilation tail, and thus have relatively large $m_{1/2}$, essentially to ensure $m_h \geq 113$ GeV. For this reason, this value of $\tan\beta$ is now disfavoured by

[9] The central regions of the direct H, A annihilation channels in Figs. 3c,d are also allowed, as the relic density is very small there. However, the exact position of this region is sensitive to the input parameters, as the cosmological fine-tuning measure Δ^Ω indicates

[10] We discuss this point again in Sect. 6

$g_\mu - 2$. It would be possible to choose a smaller value of $m_{1/2}$ if one made greater allowance for theoretical error in the m_h calculation, e.g., by choosing $m_t > 175$ GeV and $A_0 > 0$, and relaxing the $g_\mu - 2$ constraint. We note that, when $\mu < 0$, consistency with the Higgs limit would have required $m_{1/2} > 830$ GeV, and we do not consider this limited region for further study.

B: This point with $\tan\beta = 10$ has much smaller $m_{1/2}$, and hence $m_h < 113$ GeV in our nominal `FeynHiggs` calculation. Though it formally fails the Higgs mass bound, it does so just barely: $m_h = 112$ GeV for this point, which is compatible with LEP [4] within the theoretical errors. On the other hand, it satisfies the $g_\mu - 2$ constraint within about one σ. Thus points A and B take complementary points of view concerning these two constraints.

C: This second point with $\tan\beta = 10$ is compatible with $g_\mu - 2$ at the 2-σ level, as well as with $m_h = 113$ GeV in our nominal `FeynHiggs` calculation. It is therefore intermediate in philosophy between points A and B.

D: Again with $\tan\beta = 10$, but one of just two points with $\mu < 0$. This point has $g_\mu - 2$ within about 3 σ of the current experimental value. Like point C, it is compatible with $m_h = 113$ GeV according to `FeynHiggs`. Note that the effect of the $b \to s\gamma$ limit is similar to that of the Higgs limit over the range of m_0 favoured by the relic density. Both constraints force this point into the coannihilation region.

E: The first of two 'focus-point' models with large m_0 at $\tan\beta = 10$. Note that `SSARD` uses $m_t = 171$ GeV for this and the other focus point, whereas the `ISASUGRA 7.51` version uses $m_t = 175$ GeV. For this reason, `FeynHiggs` yields somewhat different values of $m_h = 112, 116$ GeV, respectively. Both of these are compatible with the LEP lower limit, taking into account theoretical uncertainties. With `SSARD`, focus-point solutions could also be obtained with the default choice of $m_t = 175$ GeV, but at larger m_0 for the same value of $m_{1/2}$.

F: This second focus-point model has larger $m_{1/2}$ and m_0, and so has a higher Higgs mass: $m_h = 115, 121$ GeV for the `SSARD` and `ISASUGRA 7.51` versions. Like point E, this point uses $m_t = 171$ GeV. Both points are about 2.5 σ away from the central value of $g_\mu - 2$. We note that the focus-point region extends to larger $m_{1/2}$ (and m_0).

G: One of two points with moderate $\tan\beta = 20$, this one is chosen to have the relatively low value $m_h = 114$ GeV. It is also just consistent with the $b \to s\gamma$ constraint, and agrees with the $g_\mu - 2$ measurement at the 1-σ level.

H: A second point with the same moderate $\tan\beta = 20$, but this time at the end point of the coannihilation 'tail' with very large $m_{1/2}$. Correspondingly, it has a larger Higgs mass: $m_h = 121$ GeV, and a small value of $g_\mu - 2$, about 2.5 σ from the central experimental value. The small $m_{\tilde{\tau}_1} - m_\chi$ mass difference has its own interesting features and challenges, as we discuss later.

I: A very ($g_\mu - 2$)-friendly point at large $\tan\beta = 35$. Note that the inclusion of one-loop corrections to m_χ are essential here. If they are not included, this point has $\tilde{\tau}_1$ as the LSP. The $b \to s\gamma$ constraint is the dominant one at small $m_{1/2}$ for this value of $\tan\beta$.

J: A second point with $\tan\beta = 35$ and $\mu > 0$, this time about half-way along the coannihilation 'tail' at large $m_{1/2}$, that is compatible with $g_\mu - 2$ at the 2-σ level.

K: One of two points in a rapid $\chi\chi \to H, A$ annihilation 'funnel', and one of just two points with $\mu < 0$. This point has $\tan\beta = 35$, which is (almost) the largest value where we find consistent electroweak vacua for this sign of μ, with our default choices of the auxiliary parameters m_t, m_b and A_0. It is far from saturating the experimental constraints, apart from $g_\mu - 2$. We note that the rapid-annihilation 'funnel' also extends to larger $m_{1/2}$ (and m_0).

L: One of two points with (almost) the largest value of $\tan\beta = 50$ for which we find consistent electroweak vacua for $\mu > 0$. This point lies in the ($g_\mu - 2$)-friendly 'bulk' of the cosmological region, and is highly compatible with the other experimental constraints.

M: A second point in a rapid $\chi\chi \to H, A$ annihilation 'funnel', again for (almost) the largest value of $\tan\beta = 50$ allowed for $\mu > 0$ with our default choices of the auxiliary parameters. This point has small $g_\mu - 2$, but satisfies all the other experimental constraints.

It is characteristic of all the solutions that the lightest Higgs strongly resembles a Standard Model Higgs boson, whilst the other Higgses are heavy and nearly degenerate in mass. The LSP is in all cases almost a pure $\tilde{B}$, except in the focus-point cases, where a non-negligible $\tilde{H}$ component is also present.

4 Theoretical uncertainties and comparisons between codes

Our proposed benchmark points were chosen using the code `SSARD` [25] to run all the input parameters down to the electroweak scale, impose the electroweak symmetry-breaking conditions there, and evaluate the physical chargino and neutralino masses including one-loop radiative corrections, which are generally $\mathcal{O}(5)\%$. This code does not include the one-loop corrections to slepton masses, which are generally $\mathcal{O}(1)\%$, taking values that increase with $\tan\beta$ and decrease with $m_{\tilde{\tau}_1}$ [33]. As mentioned earlier, the `FeynHiggs` code [30] is used to evaluate the Higgs spectra.

Some words of caution are in order. There are several available programs for calculating the supersymmetric particle spectrum and computing the physical observables considered in this paper. In general, these programs use different algorithms and, depending on their purpose, may have different levels of sophistication. The magnitudes of the resulting differences depend on the particular observable considered, on whether the results are expressed as functions of GUT-scale input parameters or

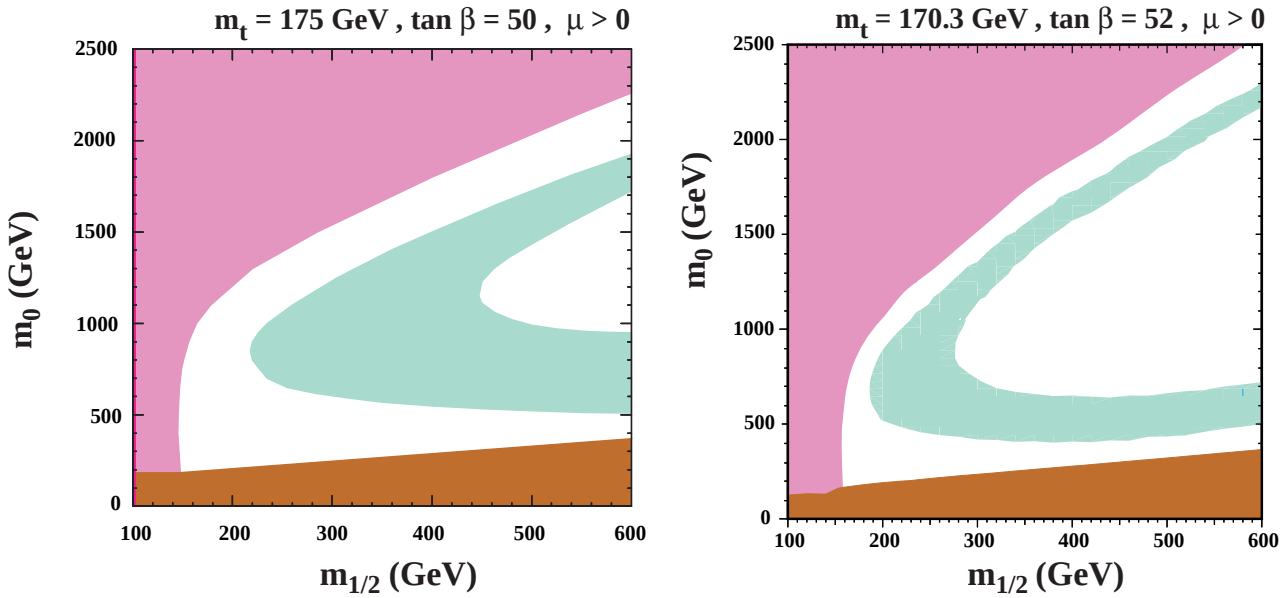

Fig. 4. *Left:* the cosmologically preferred region obtained with `Neutdriver` [70] and mass spectra from the `BMPZ` code [33], for the same parameters as in Fig. 3d. *Right:* the corresponding result from `SSARD`, but for $\tan\beta = 52$ and $m_t = 170.3$ GeV

physical masses, etc.. For example, in Fig. 4a we show the cosmologically preferred region [17] which was obtained with `Neutdriver` [70] and mass spectra from the `BMPZ` code [33], for the same parameters as in Fig. 3d. We can see that the relic densities found for the same values of $m_{1/2}$ and m_0 can be quite different, reflecting in part the sensitivity Δ^{Ω} (7) [24] noted earlier, which is generally larger at large $\tan\beta$[11]. In Figs. 3d and 4a, there are points at intermediate values of m_0 and $m_{1/2}$ where the results for $\Omega_\chi h^2$ can differ by as much as a factor of 20. We have sought to understand the origin of this apparent discrepancy and the related theoretical uncertainty in the calculations.

Comparing codes, we find that the bulk of the effect is due to differences in the supersymmetric mass spectrum, most notably the values for the CP-odd Higgs mass m_A and the μ parameter. We remind the reader that although both `SSARD` and `BMPZ` are NLO programs, numerical differences do arise at NNLO due to a different treatment of the NNLO terms. We list some of these effects below:

- The treatment of gauge coupling unification. In `SSARD`, all three gauge couplings are unified at the GUT scale, and the resulting prediction for the weak scale value of α_s is shown in Table 1. On the other hand, in `BMPZ` (`ISASUGRA`), α_s is treated as an input at the weak scale, with the following values: $\alpha_s = 0.119$ (0.118). The three gauge couplings do not in general unify, and model-dependent GUT-scale threshold corrections are assumed to account for the mismatch. This difference in the value of α_s affects the evolution of λ_t between m_Z and m_{GUT}, as well as the extraction of λ_b from $m_b(m_b)$.
- Differences in the extraction of $\lambda_t(m_Z)$, which amount to a $\sim 2.5\%$ effect. Most of this uncertainty comes from using the running top quark mass (`SSARD`) versus the pole mass (`BMPZ`) as an argument in the one-loop correction to m_t[12]. Given that the one-loop correction to m_t is typically about 11%, the resulting differences in λ_t are well within the NNLO uncertainty, but have a major impact (up to $\sim 30\%$ at large m_0) on the extracted value of the μ parameter.
- Imposing electroweak symmetry breaking. One can choose to minimize the effective potential at the scale m_Z (`SSARD`), or at the scale of the average stop mass $Q = \{m_{\tilde{t}_1} m_{\tilde{t}_2}\}^{1/2}$ (`BMPZ and ISASUGRA`). In the former case, care is taken to include corrections $\mathcal{O}(\ln(Q/m_Z))$, in order to avoid spurious differences in the values of the μ parameter, which affects the gaugino-higgsino mixing and the pseudoscalar mass m_A. The latter has a major effect in regions where s-channel annihilation through A exchange is dominant.
- Computation of the Higgs sector. All of the effects already mentioned have an impact on the calculation of the Higgs boson masses. Furthermore, `SSARD` uses the results of [29], which include some two-loop effects, while `BMPZ and ISASUGRA` apply the one-loop Higgs mass corrections [33] at the scale Q. The m_A calculation is also affected by numerical differences in the extracted values of λ_b. Altogether, we find that the values for m_A in the two cases can differ by as much as $\sim 20\%$.

[11] The results of [20] are not so dissimilar from those of [22]. We are aware of other calculations underway (G. Bélanger, F. Boudjema, A. Djouadi, M. Drees, A. Lahanas and L. Roszkowski, private communications), which also give rather diverse answers

[12] Both `BMPZ` and `SSARD` include the SM two-loop $\overline{\rm MS}$ contribution [71], assuming it is close to the $\overline{\rm DR}$ value

Differences of such magnitudes are usually not important for collider phenomenology. However, this is not the case with the relic density calculation at large values of $\tan\beta$, because of the high sensitivity (7). Recall that then the dominant annihilation channel is s-channel A exchange into bottoms, and that the annihilation cross section scales as

$$\sigma \sim \frac{m_\chi^2 m_b^2}{m_W^2(4m_\chi^2 - m_A^2)^2} N_1^2 N_3^2 \tan^2\beta, \qquad (9)$$

where $N_{1,3}$ are the Bino and Higgsino components of the LSP. The product $N_1 N_3$ is relatively large when $(|\mu| - M_1)^2 \lesssim M_Z^2$. It is easy to see that in regions of parameter space where one is not very far away from the A pole, and μ is not very large, the $\sim 20\%$ effects in m_A and μ can combine to an ~ 10 effect in the $\Omega_\chi h^2$ calculation.

It is possible to vary slightly the input parameters and obtain reasonable agreement for the spectra obtained using `SSARD` and `BMPZ/ISASUGRA 7.51`. Panel (b) of Fig. 4b shows the cosmologically preferred dark matter region obtained with `SSARD` using slightly different inputs: $\tan\beta = 52$ and $m_t = 170.3$ GeV. We now see improved agreement (to within a factor of 2) between Figs. 4a and b. We have isolated several factors that contribute to this remaining difference, all of them related to the dark matter calculation. One is the treatment of the bottom-quark radiative corrections and bottom-quark mass, whose treatment in `SSARD` was discussed in [22]. `Neutdriver` typically uses a higher value of m_b, which leads to a lower relic density. `Neutdriver` also does not integrate the Boltzmann equations, but uses an analytic approximation [6] based on non-relativistic expansions of the annihilation cross sections. Other code differences concern the extent to which coannihilation effects are included, and the treatment of s-channel annihilation rates. Therefore, in comparing results over the CMSSM parameter plane, one must be sure not only to understand the differences in the spectrum codes, but also those in the codes used to calculate the relic density.

The above discussion has focused on CMSSM spectra produced by two fully NLO codes, and we have seen that in spite of the present theoretical uncertainties, relatively well-matched spectra can be obtained, e.g., by varying the input parameters. Although very versatile, the codes generally available for Monte Carlo simulations of supersymmetry, such as `ISASUGRA` [26], `SPYTHIA` [72] and `SUSYGEN` [73], do not always include all of the ingredients of a complete NLO analysis. For example, all three programs so far lack the one-loop radiative corrections to the chargino and neutralino masses[13]. For the convenience of the experimental simulations that frequently use one of these codes, we have made searches in the input parameter space of `ISASUGRA 7.51` to find points that reproduce specific features of the spectra of the different models shown in Table 1. In some cases, significant differences are inevitable, and compromises have been made. The non-implementation of radiative corrections to the chargino and neutralino masses is a particular snag, and we hope that this can be overcome in future issues of `ISASUGRA`, `SPYTHIA` and `SUSYGEN`. The `ISASUGRA` parameters that best reproduce the most relevant features of the spectra of Table 1 are shown in Table 3, and we use them for the discussion of decay signatures in this Section. Despite these differences, we note that the general agreement between our calculated spectra and those generated by `ISASUGRA 7.51` is good[14]. The most severe differences occur in the focus-point region and at large $m_{1/2}, m_0$ at large $\tan\beta$. We note in passing some of the problems that arise when trying to match `ISASUGRA 7.51` spectra.

For this purpose, it is convenient to separate the proposed benchmarks into three classes of points.

- Points in the 'bulk' and the coannihilation 'tail'. Here the most relevant masses to fit are those of the lightest neutralino χ and the lightest stau $\tilde{\tau}_1$, since the other particles are less relevant for the dark matter calculation. It is easy to fit m_χ and $m_{\tilde{\tau}_1}$ by varying just $m_{1/2}$ and m_0: one first varies $m_{1/2}$ to fit the neutralino mass and then adjusts m_0 to fit the stau mass. In these cases, the most relevant fact is that `ISASUGRA 7.51` does not include the one-loop corrections to the neutralino and chargino masses, and hence returns lower neutralino masses for the same input values of m_0 and $m_{1/2}$. In order to compensate for this, one has to crank $m_{1/2}$ up in order that the tree-level mass from `ISASUGRA 7.51` looks like the one-loop-corrected mass. However, the stop masses also depend strongly on $m_{1/2}$, and therefore increase when this is done, as can be seen by comparing Tables 1 and 3. In turn, once the stop masses are higher, the Higgs mass also increases, as also seen in Table 3. It would, in principle, be possible also to vary the other input parameters so as to improve the match, but there is no well-defined procedure for doing this, and it is not clear what would be learned from such a lengthy exercise. Since the rest of the spectrum has intrinsic uncertainties anyway, we have not striven for perfect matches[15].
- Focus points. These points are basically defined by the LSP mass and a certain value for the gaugino-higgsino mixing, which is in turn determined by the ratio of the one-loop corrected values of the $U(1)$ gaugino mass M_1, and μ. Here, the absence of one-loop corrections in `ISASUGRA 7.51` is again unfortunate. In these cases, we have tried to match the masses of the LSP and χ_2^0, since they correspond to similar values of the effective M_1 and μ values. Here again, we vary only a couple of parameters: $m_{1/2}$ and m_0, which determines μ and therefore the χ_2^0 mass. The change in m_0 alters the

[13] These are important not only for relating physical masses to GUT-scale input parameters, but also for relating searches for sparticle species, e.g., $e^+e^- \to \chi^+\chi^-$ and $\chi_1^0\chi_2^0$

[14] For example, for the *same* input parameters, the percent difference is generally not larger than 2% across the sparticle spectrum. The biggest differences (10-20%) are found for the heavy Higgs masses for points K, L and M

[15] We note in passing that it was necessary to fix a minor glitch in `ISASUGRA` 7.51 in order to find a solution for point H. We are grateful to I. Hinchliffe and F. Paige for their help

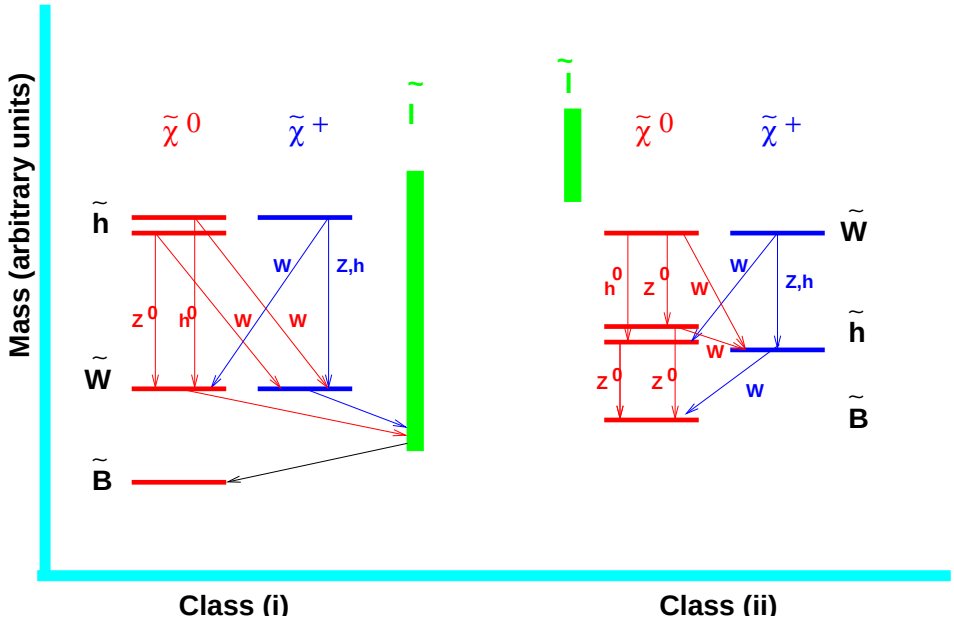

Fig. 5. Characteristic features of the spectra and principal decay modes in the two classes of benchmark points

slepton masses by about 50 GeV, as seen by comparing Tables 1 and 3.
– Points in the rapid $\chi\chi \to A, H$ annihilation region. In these cases, the relevant masses are $m_{1/2}$ and m_A. The first can still be fit, but m_A is only a very slowly varying function of m_0. Since m_A varies more rapidly with $\tan\beta$, we vary this parameter instead. For convenience, since we use a lower value of $\tan\beta$ for point M, we use it for point L as well.

At the end of this lengthy discussion, it should be clear that the benchmark points are defined by the physical spectrum and not the values of m_0, $m_{1/2}$, $\tan\beta$ etc., which are attached to them. The latter are nothing but convenient labels, which may vary from one program to another. In view of its versatility, in the rest of this paper, we use `ISASUGRA` to discuss sparticle decays and experimental signatures. The physics, of course, should remain unchanged, as long as the physical spectrum is the same. We stress that most of the differences discussed above are higher-order effects and represent in part the theoretical uncertainty in the calculation of the sparticle spectrum.

5 Decay branching ratios

The decay branching ratios in all the proposed scenarios have been evaluated using the program `ISASUGRA 7.51`. The benchmark points can be subdivided roughly into two classes, distinguished by the organization of their particle masses and their dominant decay modes. The most salient features of the decay signatures are displayed in Fig. 5, and can be summarized as follows.

(i) For points A-D and G-M, we find that $|\mu| > M_2$, which has the following consequences:

– The χ_i^0 mass sequence starts as $\tilde{B}^0$, $\tilde{W}^0$ with some admixture of $\tilde{H}^0_{1,2}$. The remaining two states are mainly a combination of the two Higgsinos with some admixture of $\tilde{W}^0$, a pattern typical of the gaugino region. Furthermore, $m_0 \leq m_{1/2}$, giving at least one slepton lighter than the χ_2^0 and $\chi_1^\pm$, and frequently several.
– The χ_2^0 decays mostly to $\tilde{\ell}\ell$ and $\tilde{\nu}\nu$ and the $\chi_1^\pm$ to $\tilde{\ell}\nu$ and $\tilde{\nu}\ell$. These decays are followed in most cases by $\tilde{\ell} \to \ell\chi_1^0$.
– The χ_3^0 and χ_4^0 decay in $50-60\%$ of the cases into $\chi_1^\pm + W^\mp$. Other principal decays are about $20-30\%$ $\chi_3^0 \to \chi_2^0 Z^0$ and about $15-25\%$ $\chi_4^0 \to \chi_2^0 h^0$.
– The $\chi_2^\pm$ decays about equally into $\chi_2^0 + W^\pm$, $\chi_1^\pm + Z^0$ and $\chi_1^\pm + h^0$.
– The squarks are in all cases heavier than any of the gauginos or sleptons and gluinos are heavier than squarks. They usually have large branching ratios for cascade decays.

These benchmark points are therefore characterized by a large proportion of final states with leptons (plus jets).

(ii) For points E and F, corresponding to the focus-point scenario, we find $M_1 < |\mu| < M_2$, with the following consequences:

– The neutralino mass sequence is roughly: $\chi \sim \tilde{B}^0$, $\chi_2^0 \sim \tilde{h}^0$, $\chi_3^0 \sim \tilde{h}^0$, $\chi_4^0 \sim \tilde{W}^0$, but with large mixing among the states. As $m_0 \gg m_{1/2}$, all sfermions are considerably heavier than the gauginos.
– The dominant neutralino decays are $\chi^0_{2,3} \to \chi_1^0 + Z^0$, $\chi^0_{3,4} \to \chi_1^\pm + W^\mp$, and to a smaller extent $\chi_4^0 \to \chi_2^0 + Z^0$ or $\chi_3^0 + h^0$.
– For chargino decays, we find $\chi_1^\pm \to \chi_1^0 + W^\pm$ with essentially a 100% branching ratio, and $\chi_2^\pm \to \chi^0_{2,3} + W^\pm$ or $\chi_1^\pm + Z^0$ or $\chi_1^\pm + h^0$.

The dominance of decays involving $W^\pm$ or Z^0 leads to final states with mainly jets and rarely leptons. These points all have a gluino lighter than the squarks.

Table 3. Mass spectra in GeV for CMSSM models calculated with `ISASUGRA 7.51`. The renormalization-group equations for the couplings and the soft superymmetry-breaking parameters include two-loop effects, and the dominant one-loop supersymmetric threshold corrections to the third generation Yukawa couplings are included. The Higgs potential is minimized at the scale $Q = (m_{\tilde{t}_1} m_{\tilde{t}_2})^{1/2}$. The Higgs and gluino masses are calculated at one loop. The rest of the superpartner spectrum is calculated at tree level at the scale Q. The input parameters have been adjusted so that the spectra best approximate those shown in Table 1. We have used the `ISASUGRA 7.51` default values $m_b^{pole} = 5$ GeV and $\alpha_s(m_Z) = 0.118$. It is assumed that $A_0 = 0$, $m_t = 175$ GeV

Supersymmetric spectra calculated using `ISASUGRA 7.51`

Model	A	B	C	D	E	F	G	H	I	J	K	L	M
$m_{1/2}$	613	255	408	538	312	1043	383	1537	358	767	1181	462	1953
m_0	143	102	93	126	1425	2877	125	430	188	315	1000	326	1500
$\tan\beta$	5	10	10	10	10	10	20	20	35	35	39.6	45	45.6
sign(μ)	+	+	+	−	+	+	+	+	+	+	−	+	+
A_0	0	0	0	0	0	0	0	0	0	0	0	0	0
m_t	175	175	175	175	175	175	175	175	175	175	175	175	175
Masses													
$\|\mu(Q)\|$	768	343	520	662	255	548	485	1597	454	876	1213	560	1842
h^0	116	113	117	117	116	121	117	124	117	121	123	118	125
H^0	893	387	584	750	1435	2955	521	1813	431	851	1070	472	1737
A^0	891	386	583	749	1434	2953	521	1812	430	851	1069	471	1735
$H^\pm$	895	394	589	754	1437	2956	527	1815	440	856	1074	481	1739
χ_1^0	252	98	164	221	119	434	154	664	143	321	506	188	854
χ_2^0	467	179	303	414	197	546	285	1217	265	594	932	349	1558
χ_3^0	770	349	524	667	262	551	491	1599	460	879	1215	564	1843
χ_4^0	785	370	540	674	317	845	506	1608	475	889	1225	578	1855
$\chi_1^\pm$	467	179	303	414	193	537	285	1217	265	594	932	349	1558
$\chi_2^\pm$	784	370	540	676	317	845	506	1608	476	890	1225	579	1855
$\tilde{g}$	1357	606	932	1203	804	2372	880	3186	828	1669	2516	1051	4029
e_L, μ_L	435	206	293	383	1433	2942	290	1092	308	599	1260	450	1957
e_R, μ_R	271	145	182	239	1427	2897	194	709	234	425	1088	370	1658
ν_e, ν_μ	428	190	282	375	1431	2941	278	1089	298	593	1258	443	1955
τ_1	269	137	175	233	1415	2873	166	664	159	334	931	242	1249
τ_2	435	209	295	384	1427	2930	296	1081	319	589	1204	439	1809
ν_τ	428	189	281	374	1425	2929	275	1076	285	571	1197	409	1803
u_L, c_L	1211	546	833	1075	1519	3397	789	2834	756	1508	2398	978	3789
u_R, c_R	1167	529	803	1036	1515	3360	764	2716	732	1452	2315	948	3643
d_L, s_L	1214	552	837	1078	1521	3398	793	2835	760	1510	2400	982	3790
d_R, s_R	1161	531	801	1032	1515	3356	762	2703	730	1445	2305	945	3631
t_1	940	400	635	845	987	2401	601	2288	569	1190	1883	744	3016
t_2	1172	580	830	1039	1292	2967	785	2649	742	1405	2122	918	3378
b_1	1126	503	769	998	1281	2961	713	2619	647	1335	2053	819	3308
b_2	1161	534	803	1028	1503	3333	762	2667	725	1406	2121	913	3388

The above summary lists only the gross features of the benchmark points and, within the two classes of models, the individual points show important differences and will sometimes (e.g., solution K) deviate in significant details from the above statements. Taken together, the benchmarks cover a large variety of cases.

Some examples of supersymmetric spectra in specific models are shown in Fig. 6. Point C is in the 'bulk' of the cosmological region, in this case for $\tan\beta = 10$ and $\mu > 0$, point E is in the focus-point region at large m_0, also for $\tan\beta = 10$ and $\mu > 0$, point J is in the coannihilation 'tail' for $\tan\beta = 35$ and $\mu > 0$, and point M is in the rapid-annihilation 'funnel' for $\tan\beta = 50$ and $\mu > 0$. Overviews of the dominant decay branching ratios of the various sparticles in these models are shown in Figs. 7 and 8.

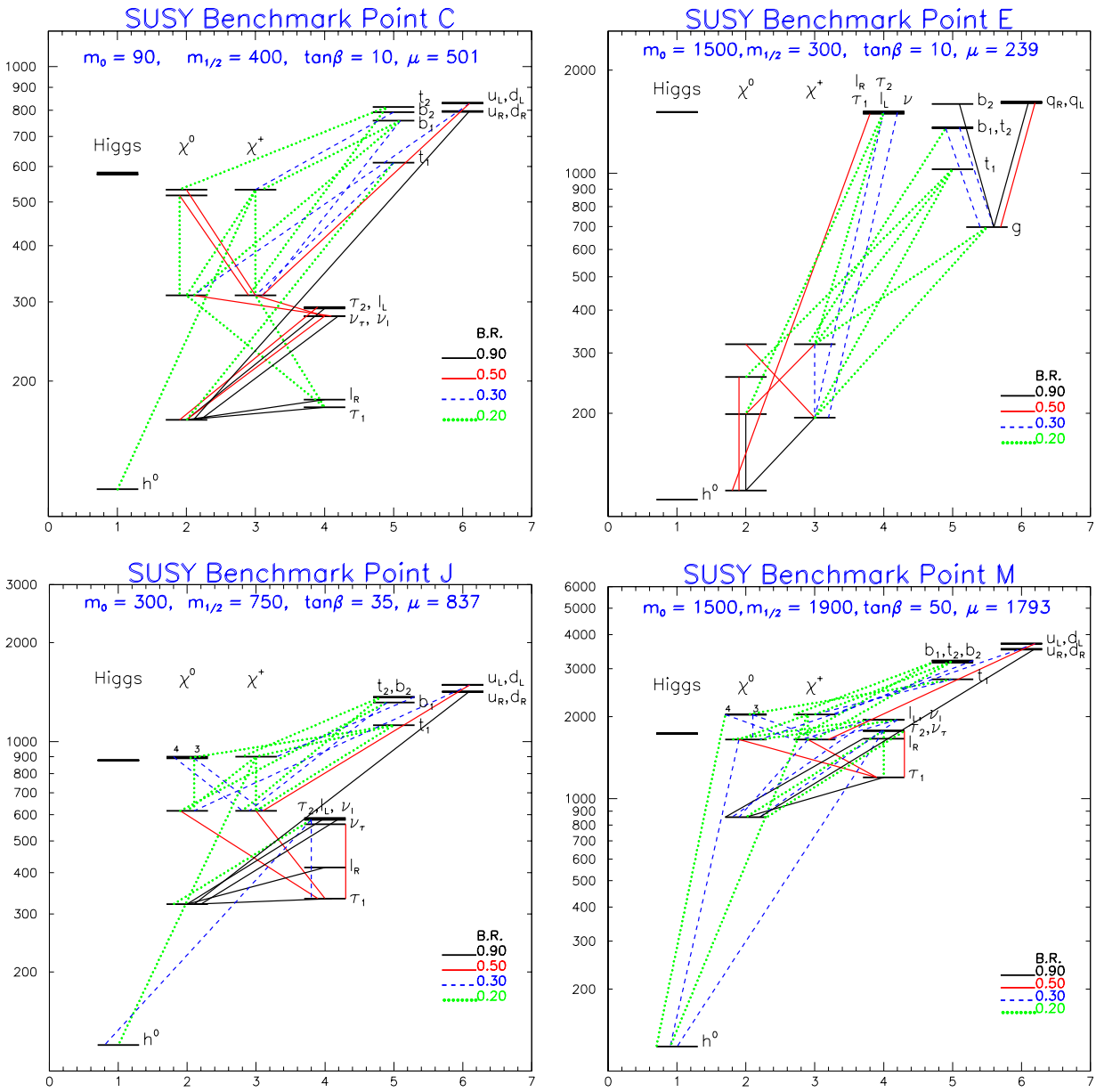

Fig. 6. The supersymmetric spectra and principal decay modes for benchmark points C,E,J and M, calculated using `ISASUGRA 7.51`

6 Prospective supersymmetric physics with different accelerators

Estimates of the numbers of CMSSM particles accessible to different accelerators in the various proposed benchmark scenarios are summarized in Fig. 9. Caution should be used in the interpretation of this figure, because it does not capture the different qualities of the measurements at different colliders. For example, the masses and decay modes of weakly-interacting sparticles and Higgs bosons can be measured more precisely at e^+e^- colliders than at the LHC, if they are kinematically accessible. Recall also that we have not chosen the points such that they give a fair representation of the more and less likely regions in the parameter space, but rather have opted to span the points over as large and diverse a region as possible, to allow studies of the consequences at the different colliders. Moreover, many of the sensitivities assumed require verification and refinement by future detailed studies. Hence Fig. 9 as such cannot be used to estimate if a particular collider would do well or not in discovering and measuring supersymmetry, but rather illustrates the diversity of a fraction of the possible scenarios and the complementarity of the different colliders.

The proposed benchmark points are ordered in Fig. 9 according to their degrees of compatibility with the recent measurement of $g_\mu - 2$. Thus, if this measurement is confirmed as evidence for physics beyond the Standard Model,

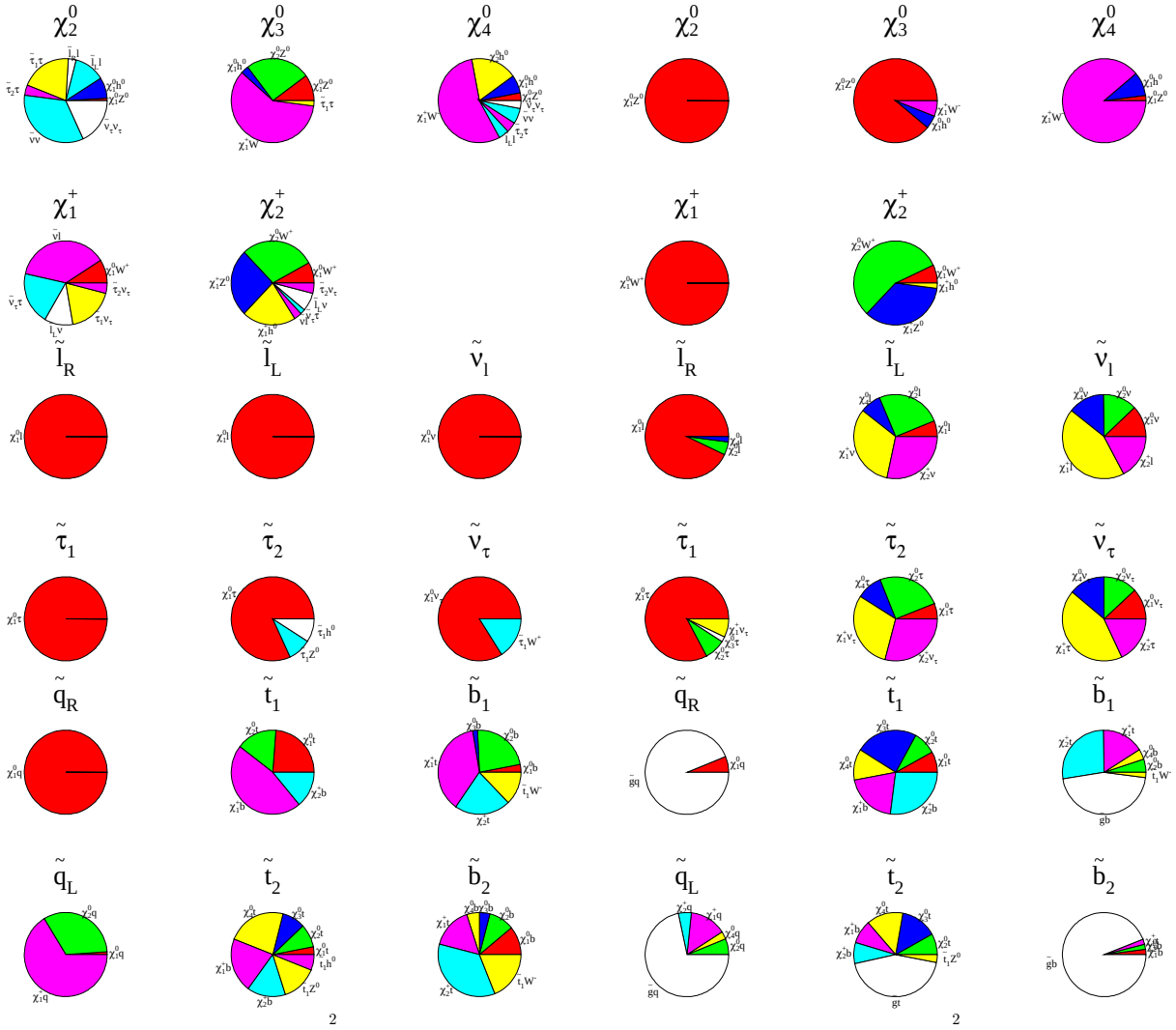

Fig. 7. Details of the principal decay branching ratios for sparticles in benchmark points C and E, calculated using `ISASUGRA 7.51`

the reader can see immediately which benchmark scenarios are preferred, and how the prospects evolve for the different accelerators considered. One may also disfavour some of the benchmark points because of the amounts of hierarchical and/or cosmological fine-tuning they require, which we have documented in Table 2.

6.1 Tevatron

The Fermilab Tevatron has just begun its next run, which is planned to deliver 1 fb^{-1} of data per experiment per year in its first two years, followed by a short shutdown for detector maintenance and luminosity upgrade. In the subsequent years, the Tevatron experiments are hoping to collect as much as 5 fb^{-1} of data per experiment per year, which might be enough for a Higgs (or supersymmetry) discovery at the dawn of the LHC. We now assess the prospects for these searches in the context of our proposed benchmark scenarios.

– The search for the Higgs boson of the Standard Model is the cornerstone of the Tevatron Run II program. A considerable amount of effort has been put into optimising the Higgs discovery channels. The Higgs discovery reach in Run II is summarized in [68]. Based on the current expectations for the performance of the new detectors, 3-σ evidence for (5-σ discovery of) a Standard Model Higgs boson with a mass of 125 GeV is possible with somewhat less that 10 (30) fb^{-1}. Similar conclusions apply to the lightest CP-even Higgs boson of the MSSM, in the decoupling limit $m_A >> m_Z$, and also for the CMSSM. Therefore, according to the Tevatron study [68], this machine will be able to discover the light Higgs boson h^0 in all of the benchmark points.
– In certain models with very light superpartners, the Tevatron also has a shot at finding supersymmetry [74]. The gold-plated mode for supersymmetry discovery at the Tevatron is the clean trilepton channel $3\ell \not{E}_T$. The corresponding reach has been recently re-

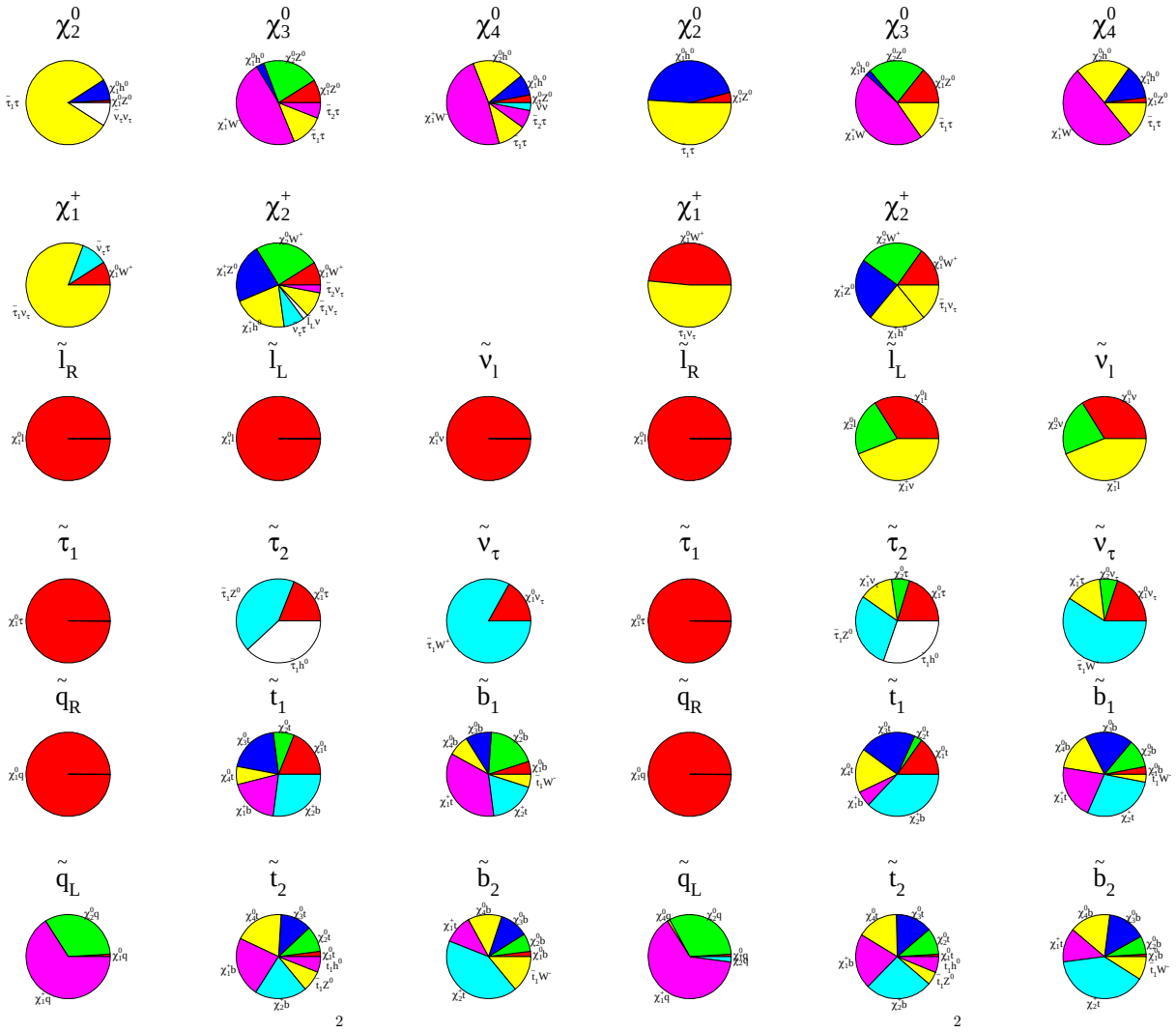

Fig. 8. Details of the principal decay branching ratios for sparticles in benchmark points J and M, calculated using `ISASUGRA 7.51`

evaluated in [75,76], with improved background estimates and optimized analysis cuts. In the case where the two-body decays of $\tilde{\chi}_1^+$ and $\tilde{\chi}_2^0$ to first generation sleptons are open, the 3-σ reach extends up to about $m_{1/2} \sim 250$ GeV. Point B therefore appears to be on the edge of the Tevatron sensitivity in this channel. However, by combining several additional channels, e.g., the like-sign di-lepton channel [77,75], the di-lepton plus tau jet channel [78,79], or the channels with jets, $\not\!\!E_T$ and isolated leptons [80], as well as data from both collaborations, point B might be observable with the full data set. In all the other 12 cases, however, the superpartners are too heavy to be abundantly produced at the Tevatron, and will escape detection. We should note that to date there have been no dedicated studies of the Tevatron chargino/neutralino reach in the focus-point region, where *both* chargino states are often kinematically accessible.

– A very interesting case is illustrated by point H. The two lightest supersymmetric particles, $\tilde{\tau}_1$ and $\tilde{\chi}_1^0$, are extremely degenerate[16], and the $\tilde{\tau}_1 - \tilde{\chi}_1^0$ mass gap is smaller than the tau mass m_τ. This possibility can occur anywhere along the borderline of the (red) shaded regions in Figs. 2 and 3, where $m_{\tilde{\tau}_1} - m_\chi \to 0^+$. In such a case, the two-body decay $\tilde{\tau}_1 \to \tau\tilde{\chi}_1^0$ is closed, and, in the absence of lepton-flavor violation in the slepton sector, the light tau slepton predominantly decays via the four-body process $\tilde{\tau}_1 \to \ell\nu_\ell\nu_\tau\tilde{\chi}_1^0$, and is stable on the scale of the size of the detector. In that case, by looking for long-lived massive charged particles [81, 82], one can probe slepton masses up to 225 GeV. The specific example of point H falls beyond this projected sensitivity, but there exist points in the CMSSM parameter space where this signature is accessible to the Tevatron.

[16] We recall that the high level of degeneracy overcomes the kinematic suppression of the annihilation cross section due to the relatively heavy LSP mass

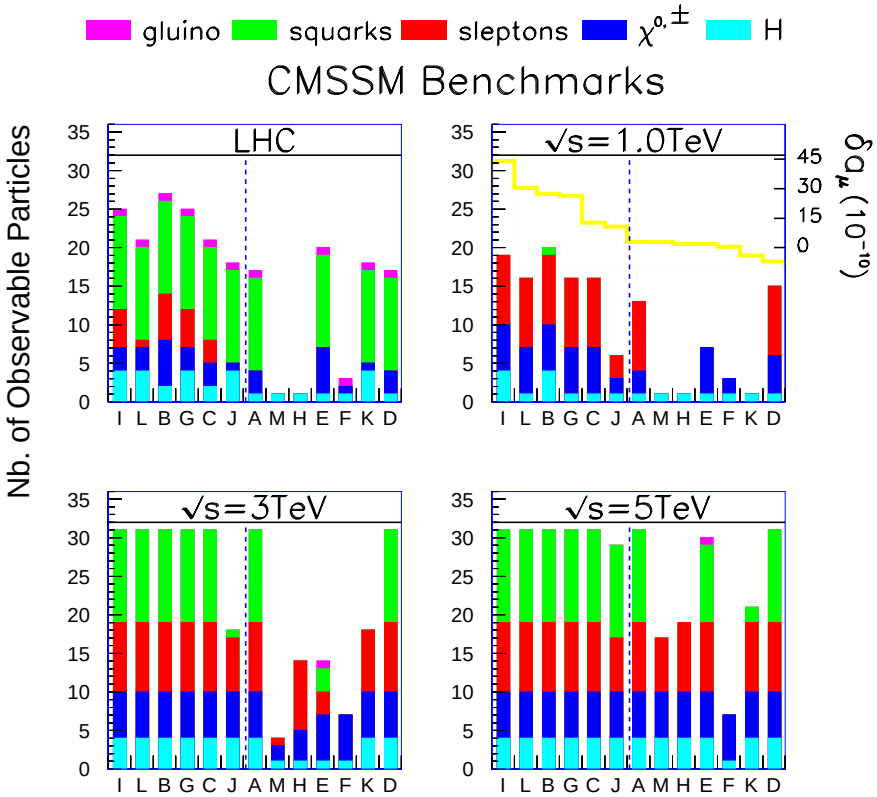

Fig. 9. Summary of the prospective sensitivities of the various accelerators considered to CMSSM production in the proposed benchmark scenarios, which are ordered by their distance from the central value of $g_\mu - 2$, as indicated by the pale (yellow) line in the second panel. We see clearly the complementarity between an e^+e^- collider and the LHC in the TeV range of energies, with the former excelling for non-strongly-interacting particles, and the LHC for strongly-interacting sparticles and their cascade decays. CLIC provides unparallelled physics reach for non-strongly-interacting sparticles, extending beyond the TeV scale. We recall that mass and coupling measurements at e^+e^- colliders are usually much cleaner and more precise than at hadron-hadron colliders such as the LHC. Note, in particular, that it is not known how to distinguish the light squark flavours at the LHC

– The lighter stop, $\tilde{t}_1$, is not within reach of the Tevatron collider for any of our proposed scenarios. However, we recall that we have always chosen $A_0 = 0$, and that $m_{\tilde{t}_1}$ may be reduced significantly for some other values of A_0 [83].

This brief discussion shows that the Tevatron collider has good prospects for discovering the lightest CMSSM Higgs boson within all our proposed benchmark scenarios, and some prospects for detecting supersymmetric particles. In particular, point B might be observed, in which case one would infer the existence of several superpartners: at least three charginos and neutralinos ($\tilde{\chi}_1^+$ and $\tilde{\chi}_2^0$, which are being produced, as well as the LSP). In addition, the observed number of events, combined with a careful examination of the lepton spectrum, may provide some information about the masses of the chargino and neutralino and hence about their leptonic branching fraction. An unusual enhancement would then also indicate the presence of light sleptons (selectrons and smuons) in the spectrum. Our benchmark points also suggest some unconventional scenarios which need to be studied in some more detail, for example the stable stau NLSP of point H and the light charginos and neutralinos with significant gaugino-higgsino mixing of point E.

6.2 LHC

A preliminary inspection has been made of the LHC potential for these benchmark points, based on the simulation results summarized in the ATLAS Physics Technical Design Report [9] and in the CMS Note [10][17]. A detailed study is clearly required before a real assessment of the LHC physics potential for these benchmarks can be made. For a preliminary look, the following assumptions were adopted to estimate the discovery potential of the LHC, assuming ATLAS+CMS combined, together with an integrated luminosity of 300 fb^{-1} per experiment.

– The light Higgs is always within reach, since its production rate and decay signatures are very similar to those in the Standard Model, as demonstrated by detailed studies of Standard Model and MSSM light Higgs bosons at LHC.
– The heavy neutral Higgses can be searched for via their decays $H^0, A^0 \to \tau\tau$ and $\mu\mu$, and the quoted $H^\pm$ discovery range is based on the decay $H^\pm \to \tau\nu$ and $\bar{b}t$. As is well known, there is a region at large m_A and moderate $\tan\beta$ where the heavier Higgs bosons may escape detection at the LHC, and this 'hole' is reflected in our results[18].
– The observation of gauginos is either through direct Drell-Yan production of $\chi_2^0\chi_1^\pm$, leading to trilepton final states, or via the inclusive production of charginos and neutralinos in the decays of squarks and gluinos. Neutralino decays to same-flavour di-leptons and missing energy yield a characteristic end point at the upper edge of the mass spectrum. If the leptonic de-

[17] Previous particle-level estimates of the LHC sensitivity can be traced from [84]
[18] Supersymmetric decays of the heavier Higgs bosons might also be an interesting signature

Table 4. Numbers of particles for each benchmark model thought to be accessible at the LHC. The observabilities we assume are obtained by extrapolating from previous simulation studies by ATLAS and CMS

	Prospective observability at the LHC												
Model	A	B	C	D	E	F	G	H	I	J	K	L	M
$m_{1/2}$	600	250	400	525	300	1000	375	1500	350	750	1150	450	1900
m_0	140	100	90	125	1500	3450	120	419	180	300	1000	350	1500
$\tan\beta$	5	10	10	10	10	10	20	20	35	35	35	50	50
sign(μ)	+	+	+	−	+	+	+	+	+	+	−	+	+
h^0, H^0, A	1	1	1	1	1	1	3	1	3	3	3	3	1
$H^\pm$	0	1	1	0	0	0	1	0	1	1	1	1	0
$\chi_i^0/\chi_j^\pm$	3	6	3	3	6	1	3	0	3	1	1	3	0
sleptons	0	6	3	0	0	0	5	0	5	0	0	1	0
squarks	12	12	12	12	12	0	12	0	12	12	12	12	0
gluino	1	1	1	1	1	1	1	0	1	1	1	1	0

cays of gauginos are enhanced because the sleptons are light, according to the published study [10], the $5-\sigma$ discovery region for χ_2^0 is bounded approximately by $m_{1/2} \leq 200$ GeV or $m_0 \leq 0.45 m_{1/2}$ for $m_{1/2} \leq 900$ GeV. However, it should be noticed that, if the squark and gluino masses are light enough to yield sufficient production rates, charginos and neutralinos with W- and Z-like branching ratios are also observable from cascade decays (which applies to points E and L). The treatment of the major background to the clean trilepton channel in those studies may now be updated along the lines of [75,76]. Heavier gaugino states are assumed observable in the same region of $(m_{1/2}, m_0)$, provided their mass is less than 450 GeV. More detailed studies are needed to assess the observability of the various gauginos for the various benchmark points, since the results depend strongly on the involved masses and decay patterns.

– The squarks have conservatively been considered observable when $m_{\tilde{q}} \leq 2500$ GeV and $m_{\tilde{t}_1} \leq 2000$ GeV. However, we note that it is not known how to distinguish the different light squark flavours at the LHC, and that the separation of squarks from gluinos needs to be studied in more detail.

– The charged sleptons can be observed through their direct production up to masses of ~ 350 GeV and perhaps indirectly in the decays of other supersymmetric particles up to masses of ~ 250 GeV. In addition, we have assumed that they are observable only if the mass differences $m_{\tilde{\ell}} - m_{\chi_1^0} \geq 30$ GeV.

– As was mentioned earlier, the $\tilde{\tau}_1$ may be long-lived, if $m_{1/2}$ and m_0 have values close to the boundary where the $\tilde{\tau}_1$ becomes the LSP, as for point H. The LHC collaborations have already made analyses of their sensitivities for such scenarios, motivated by gauge-mediated models. They have found that such a $\tilde{\tau}_1$ can be detected at the LHC by measuring delayed signals produced by these particles in the external muon spectrometers of ATLAS [85] and CMS [86], whose time resolutions are ~ 1 ns. By combining time and momentum measurements, it is possible to determine $m_{\tilde{\tau}_1}$. A mass resolution of $\sim 3.5\%$ was obtained for gauge-mediated point G2b in [9], where $m_{\tilde{\tau}_1} \sim 100$ GeV. At point H, the $\tilde{\tau}_1$ is much heavier, and its detectability requires further study.

– The sneutrinos are not counted as observable, since they have large branching ratios for invisible decays into $\tilde{\nu} \to \nu\chi_1^0$.

Our preliminary estimates of the numbers of detectable particles of each kind for each benchmark point are summarized in Table 4.

The great potential of the LHC for the discovery of squarks and the gluino as well as the lightest Higgs is clearly apparent. For most benchmark points, the discovery of some of the gauginos and sleptons would also be possible. However, it is also seen that for the points with the heaviest spectra, namely models F, H and M, the LHC may have difficulty in finding any MSSM state except the light Higgs boson. It is, however, not excluded that at least some of the states in these solutions will be found to be detectable after more detailed work has been done, as some squark masses are close to the limits chosen above. There is also the possibility of a luminosity upgrade for the LHC, which might extend its reach for squark and gluino masses up to about 3 TeV.

We have not studied in detail the extent to which the different squark flavours may be distinguished at the LHC. However, previous studies have demonstrated that in general left-handed and right-handed squarks of any generation can be disentangled on the basis of their different masses and decay modes. Also, previous work shows that the stops and sbottoms can be recognised relatively easily, because of their peculiar decay modes. There is also some hope to be able to tag charm squarks, although this has not been studied yet. The squarks corresponding to the light flavours, u, d, s, are harder to disentangle, but a measurement of the total squark production cross section would indicate that several species have been produced and may allow their number to be counted.

Previous studies [9,10] demonstrated for six benchmark points that several sparticle spectroscopic parameters could be measured with precisions of a few percent us-

Table 5. Numbers of particles accessible for each benchmark model for various lepton-antilepton collider centre-of-mass energies in TeV. Channels are considered observable when their cross section times branching ratio to visible final states exceeds 0.1 fb, taking account of the invisible final states originating from some neutralino and sneutrino decay modes. No considerations of realistic detection efficiencies have been included

Observable particles at linear e^+e^- colliders

$\sqrt{s}$	Model	A	B	C	D	E	F	G	H	I	J	K	L	M
	$m_{1/2}$	600	250	400	525	300	1000	375	1500	350	750	1150	450	1900
	m_0	140	100	90	125	1500	3450	120	419	180	300	1000	350	1500
	$\tan\beta$	5	10	10	10	10	10	20	20	35	35	35	50	50
	sign(μ)	+	+	+	−	+	+	+	+	+	+	−	+	+
1.0	Higgs	1	4	1	1	1	1	1	1	4	1	1	1	1
1.0	$\chi_i^{0,\pm}$	3	6	6	5	6	2	6	0	6	2	0	6	0
1.0	slept	9	9	9	9	0	0	9	0	9	3	0	9	0
1.0	squa	0	1	0	0	0	0	0	0	0	0	0	0	0
3.0	Higgs	4	4	4	4	1	1	4	1	4	4	4	4	1
3.0	$\chi_i^{0,\pm}$	6	6	6	6	6	6	6	4	6	6	6	6	2
3.0	slept	9	9	9	9	3	0	9	9	9	7	8	9	1
3.0	squa	12	12	12	12	3	0	12	0	12	1	0	12	0
5.0	Higgs	4	4	4	4	4	1	4	4	4	4	4	4	4
5.0	$\chi_i^{0,\pm}$	6	6	6	6	6	6	6	6	6	6	6	6	6
5.0	slept	9	7	9	9	9	0	9	9	9	7	9	9	7
5.0	squa	12	12	12	12	10	0	12	0	12	12	2	12	0
1.0	TOT	13	20	16	15	7	3	16	1	19	6	1	16	1
3.0	TOT	31	31	31	31	13	7	31	14	31	18	18	31	4
5.0	TOT	31	29	31	31	29	8	31	19	31	29	21	31	17

ing kinematic distributions. This allows the fundamental parameters of the CMSSM to be constrained to $1\%-10\%$, depending on the point studied.

6.3 Linear e^+e^- colliders up to 1 TeV

Electron-positron collisions at centre-of-mass energies up to about 1 TeV are envisaged by the TESLA [87], NLC [88,89] and JLC [90] projects. In each case, a possible first phase at energies up to about 500 GeV is also considered. In both the lower- and higher-energy phases, data samples of the order of 1000 fb^{-1} or more will be collected over a period of several years. Recent supersymmetric benchmark studies for TESLA [11] have included two CMSSM scenarios with $\tan\beta = 3$ (30), $m_0 = 100(160)$ GeV, $m_{1/2} = 200$ GeV, $\mu > 0$, and $A_0 = 0$ (600) GeV. In the case of the first point, the Higgs mass is less than 100 GeV, and thus now ruled out by LEP.

Sparticles can be produced at any linear e^+e^- collider if its centre-of-mass energy is larger than twice the mass of the sparticles, the pair production threshold, except for heavier charginos and neutralinos, which can be produced in association with the lightest chargino or neutralinos, respectively[19]. Typical supersymmetric signals are multi-lepton final states and multi-jet final states with large missing transverse energy. Sneutrinos can be detected at threshold energies if these can decay into channels including charged leptons with a sufficiently large branching ratio. For example, in some scenarios the $\tilde{\nu}_\tau$ can decay into $\tau\tilde{W}$. Otherwise, sneutrinos can be detected at higher energies via the decays of charginos. Apart from the threshold requirement to produce the particles, we require the branching ratio times cross section for the detectable channels to be larger than 0.1 fb in order to observe the sparticle, leading to at least 100 produced sparticles in the total data sample.

Table 5 shows the sparticles which can be observed at a 1 TeV linear e^+e^- collider in each of the different benchmark points proposed in this paper. The unpolarized cross sections and the decay branching ratios were computed using `ISASUGRA 7.51`. The listed numbers of observable particles take into account the decays of sneutrinos and neutralinos into undetectable final states.

We note the following points concerning searches for CMSSM particles at a linear e^+e^- collider in the energy range $\lesssim 1$ TeV.

– The lightest CMSSM Higgs boson is always detectable in a first phase even below $\sqrt{s} \sim 500$ GeV, and its mass, width, spin-parity and couplings can be measured with high precision [11]. In the second phase, interesting measurements could be made of the trilinear Higgs self-coupling. These possibilities would go far

[19] For sufficiently light neutralinos and sneutrinos, observation of the radiative production of otherwise invisible final states may be experimentally accessible

beyond the Higgs measurements possible at the Tevatron or the LHC, and could be used to constrain significantly the CMSSM parameter space. Higgs studies would form an attractive cornerstone of the first phase of a linear e^+e^- collider.

- In all the proposed scenarios except H, K and M, a number of additional sparticles is within reach of a 1 TeV linear e^+e^- collider. These exceptions are amongst those disfavoured by the measurement of $g_\mu - 2$. In approximately half of the cases, particularly those which are consistent with the $g_\mu - 2$ measurement at the 2 σ level, a large fraction of the sleptons and gauginos can be detected. In particular, points B and I are very favourable for a linear collider with centre-of-mass energy up to 1 TeV.
- The LHC and such a linear collider are largely complementary in their sparticle mass reaches. For example, in the case of point L, the linear collider would see all the sleptons, while the LHC would see all the squarks.
- In contrast to the LHC, one notices that the squarks are not generally accessible in the proposed models.
- Beyond the discovery of sparticles, a crucial issue in the understanding of the nature of any new physics observed will be the accuracy obtainable in the determination of the sparticle masses and decays, and also their quantum numbers and mixing. A strong advantage of lepton colliders is the *precision* with which such sparticle properties can be measured. Typically, the masses of sleptons and gauginos can be determined with a precision of a few per mille, by threshold scans and by measuring end points of two-body decay channel signatures in inclusive distributions. This uncanny precision, even for a limited number of sparticles, will be of cardinal importance for the reconstruction of the underlying supersymmetric model and breaking mechanism [91].
- Furthermore, the availability of polarized beams at a linear collider will provide additional tools for identifying supersymmetric particles and allow for additional measurements of parameters of the supersymmetric model, such as the mixing angles of the sparticles [92].
- In a few cases the heavy Higgs particles are within reach of a 1 TeV e^+e^- collider, but we also note that the reach for heavy Higgses can be extended with a photon collider option [93], in which the lepton beams are converted into high-energy photon beams, with a peak energy of up to 80% of the original incoming lepton beam energy. Heavy Higgses can be singly produced in two photon interactions, increasing the reach in detection to Higgs particles with masses of approximately 75-80% of the centre-of-mass energy. Such an option would be very useful for the points C, D, G and L where the heavy Higgs particles become accessible in the two-photon collider mode.
- We note also that a precise measurement of the two-photon width of the light Higgs boson, which appears feasible at a photon collider [94], might give evidence of the existence of new physics, such as supersymmetry, even if no other new particles besides the Higgs boson have been discovered at the LHC or a 1 TeV linear collider.

Panels (a) to (c) of Fig. 10 show the increasing reach for sparticles and Higgs bosons at linear e^+e^- colliders as a function of the centre-of-mass energy. In the benchmark points with a value of $g_\mu - 2$ close to the central value of the recent measurement, a 500 GeV linear collider will detect, apart from the lightest Higgs, several selectrons, charginos and neutralinos. Furthermore, for many of these scenarios, a 800 GeV linear collider will see most of the sleptons and gauginos. Heavy Higgs bosons and some of the squarks become observable for a linear collider with a centre-of-mass energy around and above 1 TeV. Panel (d) of Fig. 10 shows the new particles that could be detected and measured at the LHC and a 1 TeV linear collider, in combination. Together they cover most of the spectrum in $g_\mu - 2$-friendly models, emphasizing the complementarity of these machines.

6.4 CLIC

CLIC is a project for an e^+e^- linear collider which aims at a centre-of-mass energy of 3 TeV, upgradable to 5 TeV at a later stage. The luminosity will be about $10^{35}\mathrm{cm}^{-2}\mathrm{s}^{-1}$. To achieve this luminosity, CLIC will work in the high beamstrahlung regime [95]. The physics potential of this machine is currently being studied [96].

To obtain a first, very crude, estimate of the potential of a linear e^+e^- collider in the multi-TeV range, we have used the same criteria as in the previous section, i.e., we assume that sparticles can be detected provided their production cross section multiplied by their branching ratio to visible final states exceeds 0.1 fb[20]. CLIC is estimated to yield an integrated luminosity of about 1000 fb^{-1} in a year, of which about a third would be close to the nominal E_{CM}. Therefore, one could accumulate 1000 fb^{-1} at this nominal energy in about three years, corresponding to 100 events produced for a cross section of 0.1 fb. More accurate estimates of the CLIC sensitivity will become possible only after simulation of the signals and backgrounds. Preliminary studies indicate that, although CLIC will operate with more beamstrahlung and hence a less well-defined centre-of-mass energy than lower-energy linear colliders, there are several physics topics for which the accelerator environment is not a serious disadvantage [96].

The unpolarized cross sections and the decay branching ratios were again computed using `ISASUGRA 7.51`. The numbers of observable particles, after taking into account the decays of sneutrinos and neutralinos into undetectable final states, are also summarized in Table 5. In preparing this Table, the possibility of detecting sneutrinos from the two-body decays of charginos has been taken into account,

[20] This limiting cross section is why some sparticles are not counted as observable, even though they are kinematically accessible. For example, at 5 TeV, at point K the $\tilde{d}_R$ and $\tilde{s}_R$ have cross sections of only 0.01 fb and the $\tilde{b}_2$ only 0.04 fb, whilst at point H the $\tilde{t}_1$ is produced with a cross section of only 0.03 fb

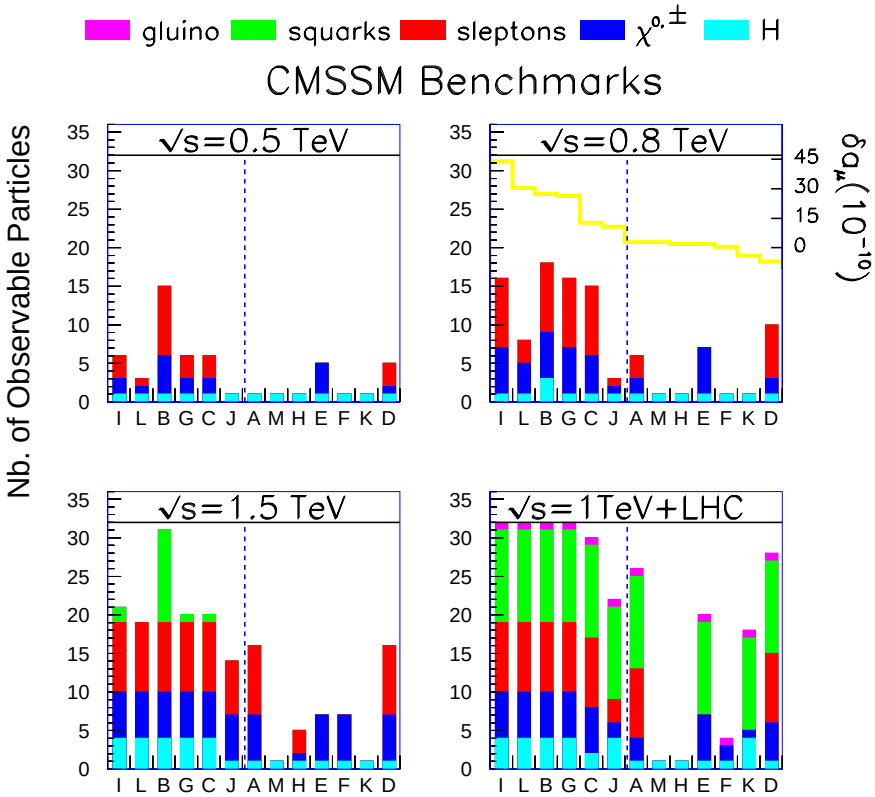

Fig. 10a–d. Summary of the prospective sensitivities of linear e^+e^- colliders with centre-of-mass energies **a** 0.5 TeV, **b** 0.8 TeV and **c** 1.5 TeV, with the 1 TeV case being shown in Fig. 9. As there, the various proposed benchmark scenarios are ordered by their distances from the central value of $g_\mu - 2$, as indicated by the pale (yellow) line in the second panel. We see clearly the gain in physics reach as the centre-of-mass energy is increased. Also shown in panel **d** are the estimated total numbers of CMSSM particles visible with the LHC and a 1 TeV linear collider combined. Together they cover most of the spectrum in $g_\mu - 2$-friendly models, emphasizing the complementarity of these machines. However, again we recall that mass and coupling measurements at e^+e^- colliders are usually much cleaner and more precise than at hadron-hadron colliders such as the LHC

and we note that, in scenario B, the sneutrinos are only observable through their associated production. Note that due to the decrease of the cross section as function of energy, the $\tilde{\nu}_\mu$ and $\tilde{\nu}_\tau$ which are observable at 3 TeV but are in principle no longer at an energy at 5 TeV if the luminosity is the same as for a 3 TeV collider. However this would ignore the fact that the machine could run at lower energy, and also the fact that CLIC makes an 'autoscan', by virtue of the beamstrahlung photon spectrum. Hence, for the counting in Table 5, these particles are considered to be detectable at a collider which can go up to 5 TeV. Finally, we note that, at point E, the gluinos are observable at energies ≥ 3 TeV, as they constitute the dominant decay mode of the squarks, but they are not listed in the Table.

Assuming that the LHC and an e^+e^- linear collider in the range $\lesssim 1$ TeV have been taking data for several years before the start of a 3 TeV machine like CLIC (CLIC3000), we infer that supersymmetry will most probably already have been discovered by that time, if it exists. Hence the rôle of CLIC may consist mainly of completing the sparticle spectrum, and disentangling and measuring more precisely the properties of sparticles already observed at the LHC and/or a lower-energy e^+e^- linear collider. However, a machine like CLIC would be needed even for the direct discovery of supersymmetry in the most problematic cases, namely scenarios H and M.

A few benchmark points emerge as typical of situations which could arise in the future.

– Point C has very low masses, and is representative also of points A, B, D, G, I, L. In these cases, LHC would have discovered the $H^\pm$, as well as seen the h^0, and also the gauginos χ_1^0, χ_2^0 and $\chi_1^\pm$, some of the charged sleptons, the squarks and the gluino. A 1 TeV linear collider would enable the detailed study of the h^0 and of the same gauginos and sleptons, and it might discover the missing sleptons and gauginos in some of the scenarios. However, one would require CLIC, perhaps running around 2 TeV, to complete the particle spectrum by discovering and studying the heavy Higgses and the missing gauginos. CLIC could also measure more precisely the squarks and in particular disentangle the left- and right-handed states and, to some extent, the different light squark flavours.

– Point J features intermediate masses, rather similar to point K. Here, the LHC would have discovered all the Higgs bosons, the squarks and the gluino, but no gauginos nor sleptons. The 1 TeV e^+e^- linear collider would study in detail the h^0 and could discover the $\tilde{e}_R$, $\tilde{\mu}_R$ and $\tilde{\tau}_1$, but other sparticles would remain beyond its kinematic reach. CLIC3000 could then study in detail the heavy Higgses. It would also discover and study the gauginos and the missing sleptons, and even observe in more detail a few of the lighter squarks that had already been discovered at LHC. However, to see the remaining squarks at a linear collider would require CLIC to reach slightly more than 3 TeV.

– Point E has quite distinctive decay characteristics, due to the existence of heavy sleptons and squarks. In this situation, the LHC would have discovered the h^0, all squarks and the gluino. The gauginos are in principle accessible, but their discovery may be made more dif-

ficult because their predominant decays are into jets, contrary to the previous benchmark points, and sleptons would remain unobserved. At a 1 TeV e^+e^- linear collider, the detailed study of the h^0 and of the gauginos could be undertaken. The discovery of the first slepton, actually a $\tilde{\nu}_e$, could be made at CLIC3000, which could also study the three lightest squarks. The discovery and analysis of the heavy Higgses would then require the CLIC energy to reach about 3.5 TeV, which would also allow the discovery of all sleptons and the observation of all squarks.

- Point M has quite heavy states, rather close to scenario H. The LHC would only discover the h^0, all other states being beyond its reach. The existence of supersymmetry might remain an open question! The 1 TeV e^+e^- linear collider also sees only the h^0, but can study it in detail, and so might provide indirect hints of supersymmetry. A CLIC3000 would be able to discover most of the gauginos and the $\tilde{\tau}_1$, but CLIC with 3.5 to 4 TeV would be required to discover the remaining gauginos and sleptons. To discover the squarks, $\ell^+\ell^-$ collisions above 6.5 TeV would be needed. There is currently no e^+e^- project aiming at such energies, and neutrino radiation becomes a hazard for $\mu^+\mu^-$ colliders at such energies.
- Point F also has heavy states. Here again, LHC sees only the h^0, but would also find the gluino. The lightest gauginos would be within the reach of a 1 TeV e^+e^- linear collider, and the heavier ones within the reach of CLIC3000. But it would only be with $\ell^+\ell^-$ collisions in the 6.5-7.5 TeV region that the heavy Higgses, the sleptons and the squarks could be found.
- As in the 1 TeV e^+e^- linear collider case, a photon collider option for CLIC would extend the discovery range for heavy Higgs bosons. It would additionally allow one to discover all four Higgs bosons in scenarios E, H and M, for a 3 TeV collider, and also in F, for a 5 TeV Collider.
- We also note that polarization would have advantages similar to those discussed earlier for a lower-energy e^+e^- linear collider.

Since assessing the viability of the CLIC technology will need at least of the order of five years more of machine studies, we assume that it will come into operation after the LHC and lower energy e^+e^- linear collider. A 3 TeV e^+e^- collider will – apart from the gluino – access as many or more sparticles as the LHC and 1 TeV linear collider combined for most scenarios, as seen by comparing Figs. 9 and 10d. However, as commented in connection with Fig. 9, a compilation such as Fig. 10d does not reflect the different level in precision of the measurements of the particle properties at the LHC and a linear collider such as CLIC. Many more precise measurements can be made with a multi-TeV lepton collider than with the LHC, which is very important for the reconstruction of the underlying supersymmetry-breaking mechanism. Higher CLIC energies, up to 5 TeV or more, could be necessary to complete the sparticle spectrum in several of the more extreme scenarios.

7 Conclusions and prospects

We have proposed some benchmarks that span the possibilities still allowed in the CMSSM, following the explorations made by LEP. A grand summary of the reaches of the various accelerators is presented graphically in Fig. 9. The different levels of shading (color) present the different types of sparticle: Higgses, charginos and neutralinos, sleptons, squarks and gluino. The first six points (I, L, B, G, C, J) are presently favoured: they are compatible within 2 σ with the present $g_\mu - 2$ measurement, and the fine tuning is relatively small for most of these points. Figure 9 summarizes the discussion of this paper and exposes clearly the complementarity of hadron and electron machines. It is apparent that many alternative scenarios need to be kept in mind.

Beyond the CMSSM framework we have discussed in this paper, one should consider more general versions of the MSSM, in which the GUT universality assumption is relaxed [97]. We note that the phenomenology of *gauge-mediated* models [12] with long-lived neutralino NLSP is very well covered by our suggested CMSSM benchmark points, whilst a charged long-lived NLSP is found for our point H. Gauge-mediated models with a promptly-decaying NLSP give rise to distinct signatures, but there are very few theoretical models that predict these. The minimal *gaugino-mediated* models [13] predict spectra [98] which are very similar to those of the benchmark points in the 'bulk' region discussed above, and are therefore to a large extent covered by our analysis. *Anomaly mediation* provides an interesting framework [14] for model building [99]. A 'phenomenological' model of anomaly mediation [100] has been incorporated in `ISASUGRA`, and might serve as a basis for future studies. Finally, we recall that *R-violating* models generally do not provide a suitable dark matter candidate, and contain so many new R-violating couplings that all the possibilities cannot be covered with only a few benchmark choices.

As we have discussed, the Tevatron has a chance to make the first inroads into the spectroscopy of the CMSSM models we have studied, with the best chance being offered by the lightest Higgs boson, followed by chargino/neutralino searches.

The LHC is expected to observe at least one CMSSM Higgs boson in all possible scenarios, and will in addition discover supersymmetry in most of the models studied. However, we do observe that the discovery of supersymmetry at the LHC is apparently not guaranteed, as exemplified by benchmarks H and M. It would be valuable to explore the extent to which precision measurements at the LHC could find indirect evidence for supersymmetry in such scenarios. We note also that, in these cases, the squarks and gluinos lie not far beyond the nominal physics reach of the LHC, and an upgrade of the luminosity to 10^{35} $\mathrm{cm}^{-2}\mathrm{s}^{-1}$ might bring them within reach.

An e^+e^- linear collider in the TeV range would in most cases bring important additional discoveries, exceptions being benchmarks H and M, and possibly E. Moreover, such a linear collider would also provide many high-precision measurements of the Higgs boson and supersym-

metric particle masses and decay modes, that would play a pivotal rôle in first checking the CMSSM assumptions and subsequently pinning down its parameters, or those of the model that supplants it. As such, it will be an essential tool for securing the supersymmetric revolution we anticipate.

In many of the scenarios proposed, the discovery and exploration of the complete set of supersymmetric particles, and especially some of the heavy Higgses, gauginos and sleptons, will have to await the advent of a machine like CLIC, which may need to run at an energy considerably higher than 3 TeV. In particular, points F and M are very challenging and would need a $\ell^+\ell^-$ collider with a centre-of-mass energy of up to 7.5 TeV in order to discover all the CMSSM particles. Distinguishing the different squark flavours could be an interesting challenge for CLIC.

If the CLIC technology cannot be extended this far, here might come a rôle for a high-energy $\mu^+\mu^-$ collider, if its neutrino radiation problems could be overcome. A lower-energy $\mu^+\mu^-$ collider would also be interesting, with its unique capabilities for Higgs measurements.

History reminds us that benchmarks have a limited shelf-life: at most one of them can be correct, and most probably none. In the near future, the CMSSM parameter space will be coming under increasing pressure from improved measurements of $g_\mu - 2$, assuming that the present theoretical understanding can also be improved, and $b \to s\gamma$, where the B factories will soon be dominating the measurements. We also anticipate significant improvement in the sensitivity of searches for supersymmetric dark matter.

We also note that astrophysical and cosmological estimates of the cold dark matter density are converging, which may improve the upper limit on $\Omega_\chi h^2$. As we mentioned earlier, lower values of $\Omega_\chi h^2$, even below 0.1, would be possible if there exists some additional form of cold dark matter. In this case, the sparticle spectrum might be somewhat lighter than in the benchmarks we propose, though the scope for this is rather limited. An interesting question for the future is whether the sparticle measurements at the LHC and particularly a linear e^+e^- collider will enable accurate calculations of $\Omega_\chi h^2$ to be made [101, 24]. This certainly seems possible in many of the benchmarks we propose, though probably not for those with very large values of Δ^Ω.

Needless to say, the preliminary observations presented above need to be confirmed by more detailed exploration of the benchmark scenarios we propose, and of any others proposed within the context of different supersymmetric model assumptions. These more detailed studies would certainly benefit from improvements in the available simulation codes. All of the necessary ingredients for a complete NLO analysis are already available [33]. In order to achieve the necessary precision, one now has to include the complete one-loop corrections to the physical particle masses as well as perform a careful treatment of sparticle thresholds, the effective potential and the Higgs boson mass parameters.

Acknowledgements. The work of K.A.O. was supported partly by DOE grant DE–FG02–94ER–40823. K.T.M. thanks the Fermilab Theory Group for hospitality during the completion of this work.

References

1. J. Ellis, S. Kelley, D.V. Nanopoulos, Phys. Lett. B **260**, 131 (1991); U. Amaldi, W. de Boer, H. Furstenau, Phys. Lett. B **260**, 447 (1991); C. Giunti, C.W. Kim, U.W. Lee, Mod. Phys. Lett. A **6**, 1745 (1991)
2. L. Maiani, Proceedings of the 1979 Gif-sur-Yvette Summer School On Particle Physics, 1; G. 't Hooft, in Recent Developments in Gauge Theories, Proceedings of the Nato Advanced Study Institute, Cargese, 1979, eds. G. 't Hooft et al., (Plenum Press, NY, 1980); E. Witten, Phys. Lett. B **105**, 267 (1981)
3. LEP Electroweak Working Group, http://lepewwg.web.cern.ch/LEPEWWG/Welcome.html
4. R. Barate et al., [ALEPH Collaboration], Phys. Lett. B **495**, 1 (2000); M. Acciarri et al., [L3 Collaboration], Phys. Lett. B **495**, 18 (2000); P. Abreu et al., [DELPHI Collaboration], Phys. Lett. B **499**, 23 (2001); G. Abbiendi et al., [OPAL Collaboration], Phys. Lett. B **499** 38. For a preliminary compilation of the LEP data presented on Nov. 3rd, 2000, see: P. Igo-Kemenes, for the LEP Higgs working group, http://lephiggs.web.cern.ch/LEPHIGGS/talks/index.html.
5. J. Ellis, D. Ross, Phys. Lett. B **506**, 331 (2001) [hep-ph/0012067]
6. J. Ellis, J.S. Hagelin, D.V. Nanopoulos, K.A. Olive, M. Srednicki, Nucl. Phys. B **238**, 453 (1984); see also H. Goldberg, Phys. Rev. Lett. **50**, 1419 (1983)
7. H.N. Brown et al. [Muon g-2 Collaboration], Phys. Rev. Lett. **86**, 2227 (2001) [hep-ex/0102017]
8. I. Hinchliffe, F.E. Paige, M.D. Shapiro, J. Soderqvist, W. Yao, Phys. Rev. D **55**, 5520 (1997)
9. ATLAS Collaboration, ATLAS detector and physics performance Technical Design Report, CERN/LHCC 99-14/15 (1999)
10. S. Abdullin et al. [CMS Collaboration], hep-ph/9806366; S. Abdullin, F. Charles, Nucl. Phys. B **547**, 60 (1999); CMS Collaboration, Technical Proposal, CERN/LHCC 94-38 (1994)
11. TESLA Technical Design Report, DESY-01-011, Part III, Physics at an e^+e^- Linear Collider (March 2001)
12. M. Dine, A.E. Nelson, Phys. Rev. D **48**, 1277 (1993) [hep-ph/9303230]; M. Dine, A.E. Nelson, Y. Shirman, Phys. Rev. D **51**, 1362 (1995) [hep-ph/9408384]; M. Dine, A.E. Nelson, Y. Nir, Y. Shirman, Phys. Rev. D **53**, 2658 (1996) [hep-ph/9507378]
13. D.E. Kaplan, G.D. Kribs, M. Schmaltz, Phys. Rev. D **62**, 035010 (2000) [hep-ph/9911293]; Z. Chacko, M.A. Luty, A.E. Nelson, E. Ponton, JHEP **0001**, 003 (2000) [hep-ph/9911323]
14. L. Randall, R. Sundrum, Nucl. Phys. B **557**, 79 (1999) [hep-th/9810155]; G.F. Giudice, M.A. Luty, H. Murayama, R. Rattazzi, JHEP **9812**, 027 (1998) [hep-ph/9810442]

15. J. Ellis, T. Falk, K.A. Olive, Phys. Lett. B **444**, 367 (1998); J. Ellis, T. Falk, K.A. Olive, M. Srednicki, Astropart. Phys. **13**, 181 (2000)
16. M.E. Gómez, G. Lazarides, C. Pallis, Phys. Rev. D **61**, 123512 (2000) [hep-ph/9907261] and Phys. Lett. B **487**, 313 (2000) [hep-ph/0004028]; R. Arnowitt, B. Dutta, Y. Santoso, hep-ph/0102181
17. J.L. Feng, K.T. Matchev, F. Wilczek, Phys. Lett. B **482**, 388 (2000) [hep-ph/0004043]
18. M. Drees, M.M. Nojiri, Phys. Rev. D **47**, 376 (1993)
19. H. Baer, M. Brhlik, Phys. Rev. D **53**, 597 (1996) and Phys. Rev. D **57**, 567 (1998)
20. H. Baer, M. Brhlik, M.A. Diaz, J. Ferrandis, P. Mercadante, P. Quintana, X. Tata, Phys. Rev. D **63**, 015007 (2001)
21. A.B. Lahanas, D.V. Nanopoulos, V.C. Spanos, Mod. Phys. Lett. A **16**, 1229 (2001), hep-ph/0009065
22. J. Ellis, T. Falk, G. Ganis, K.A. Olive, M. Srednicki, Phys. Lett. B **510**, 236 (2001), hep-ph/0102098
23. J. Ellis, K. Enqvist, D.V. Nanopoulos, F. Zwirner, Mod. Phys. Lett. A **1**, 57 (1986); R. Barbieri, G.F. Giudice, Nucl. Phys. B **306**, 63 (1988)
24. J. Ellis, K.A. Olive, Phys. Lett. B **514**, 114 (2001), hep-ph/0105004
25. Information about this code is available from K.A. Olive: it contains important contributions from T. Falk, G. Ganis, J. McDonald, K.A. Olive, M. Srednicki
26. We use version 7.51 of H. Baer, F.E. Paige, S.D. Protopopescu, X. Tata, ISAJET 7.48: A Monte Carlo event generator for pp, $\bar{p}p$, and e^+e^- reactions, hep-ph/0001086, with a couple of minor modifications, which will be implemented in the upcoming release of version 7.52
27. L.E. Ibáñez, G.G. Ross, Phys. Lett. B **110**, 215 (1982); L.E. Ibáñez, Phys. Lett. B **118**, 73 (1982); J. Ellis, D.V. Nanopoulos, K. Tamvakis, Phys. Lett. B **121**, 123 (1983); J. Ellis, J. Hagelin, D.V. Nanopoulos, K. Tamvakis, Phys. Lett. B **125**, 275 (1983); L. Alvarez-Gaumé, J. Polchinski, M. Wise, Nucl. Phys. B **221**, 495 (1983)
28. V. Barger, M.S. Berger, P. Ohmann, Phys. Rev. D **49**, 4908 (1994) [hep-ph/9311269]
29. M. Carena, J. Ellis, A. Pilaftsis, C.E. Wagner, Nucl. Phys. B **586**, 92 (2000) [hep-ph/0003180]
30. S. Heinemeyer, W. Hollik, G. Weiglein, Comput. Phys. Commun. **124**, 76 (2000) [hep-ph/9812320]
31. D. Pierce, A. Papadopoulos, Phys. Rev. D **50**, 565 (1994) [hep-ph/9312248]
32. D. Pierce, A. Papadopoulos, Nucl. Phys. B **430**, 278 (1994) [hep-ph/9403240]
33. D.M. Pierce, J.A. Bagger, K. Matchev, R. Zhang, Nucl. Phys. B **491**, 3 (1997) [hep-ph/9606211]
34. Information about this code may be obtained from G. Ganis
35. Joint LEP 2 Supersymmetry Working Group, http://lepsusy.web.cern.ch/lepsusy/Welcome.html
36. Joint LEP 2 Supersymmetry Working Group, Combined LEP Chargino Results, up to 208 GeV, http://lepsusy.web.cern.ch/lepsusy/www/inos_moriond01/charginos_pub.html
37. Joint LEP 2 Supersymmetry Working Group, Combined LEP Selectron/Smuon/Stau Results, 183-208 GeV, http://alephwww.cern.ch/~ganis/SUSYWG/SLEP/sleptons_2k01.html
38. T. Affolder et al. [CDF Collaboration], hep-ex/0106001 and references therein
39. J. Ellis, T. Falk, K.A. Olive, M. Schmitt, Phys. Lett. B **388**, 97 (1996) and Phys. Lett. B **413**, 355 (1997); J. Ellis, T. Falk, G. Ganis, K.A. Olive, M. Schmitt, Phys. Rev. D **58**, 095002 (1998)
40. H.E. Haber, R. Hempfling, A.H. Hoang, Zeit. für Phys. C **75**, 539 (1997)
41. C. Degrassi, P. Gambino, G.F. Giudice, JHEP **0012**, 009 (2000); see also M. Carena, D. Garcia, U. Nierste, C.E. Wagner, Phys. Lett. B **499**, 141 (2001) hep-ph/0010003
42. M.S. Alam et al., [CLEO Collaboration], Phys. Rev. Lett. **74**, 2885 (1995) as updated in S. Ahmed et al., CLEO CONF 99-10; BELLE Collaboration, BELLE-CONF-0003, contribution to the 30th International conference on High-Energy Physics, Osaka, 2000
43. A. Czarnecki, W.J. Marciano, Phys. Rev. D **64**, 013014 (2001) [hep-ph/0102122]
44. M. Davier, A. Höcker, Phys. Lett. B **435**, 427 (1998)
45. R.R. Akhmetshin et al., [CMD-2 Collaboration], Phys. Lett. B **475**, 190 (2000)
46. J.Z. Bai et al., [BES Collaboration], hep-ex/0102003, and references therein
47. S. Anderson et al., [CLEO Collaboration], Phys. Rev. D **61**, 112002 (2000)
48. S. Narison, Phys. Lett. B **513**, 53 (2001), hep-ph/0103199; W.J. Marciano, B.L. Roberts, hep-ph/0105056; J.F. De Troconiz, F.J. Yndurain, hep-ph/0106025; M. Davier, S. Eidelman, A. Höcker, private communication
49. P. Fayet, Unification of the Fundamental Particle Interactions, eds. S. Ferrara, J. Ellis, P. van Nieuwenhuizen (Plenum, New York, 1980), p.587
50. J.A. Grifols, A. Mendez, Phys. Rev. D **26**, 1809 (1982); J. Ellis, J. Hagelin, D.V. Nanopoulos, Phys. Lett. B **116**, 283 (1982); R. Barbieri, L. Maiani, Phys. Lett. B **117**, 203 (1982). D.A. Kosower, L.M. Krauss, N. Sakai, Phys. Lett. B **133**, 305 (1983); T.C. Yuan, R. Arnowitt, A.H. Chamseddine, P. Nath, Z. Phys. C **26**, 407 (1984); I. Vendramin, Nuovo Cim. A **101**, 731 (1989)
51. J.L. Lopez, D.V. Nanopoulos, X. Wang, Phys. Rev. D **49**, 366 (1994); U. Chattopadhyay, P. Nath, Phys. Rev. D **53**, 1648 (1996)
52. J.L. Feng, K.T. Matchev, Phys. Rev. Lett. **86**, 3480 (2001) [hep-ph/0102146]; L.L. Everett, G.L. Kane, S. Rigolin, L. Wang, Phys. Rev. Lett. **86**, 3484 (2001) [hep-ph/0102145]; E.A. Baltz, P. Gondolo, Phys. Rev. Lett. **86**, 5004 (2001) [hep-ph/0102147]; U. Chattopadhyay, P. Nath, Phys. Rev. Lett. **86**, 5854 (2001), hep-ph/0102157. S. Komine, T. Moroi, M. Yamaguchi, Phys. Lett. B **506**, 93 (2001) [hep-ph/0102204]; S.P. Martin, J.D. Wells, Phys. Rev. D **64**, 035003 (2001); H. Baer, C. Balazs, J. Ferrandis, X. Tata, Phys. Rev. D **64**, 035004 (2001), hep-ph/0103280; R. Arnowitt, B. Dutta, B. Hu, Y. Santoso, Phys. Lett. B **505**, 177 (2001) [hep-ph/0102344]
53. J. Ellis, D.V. Nanopoulos, K.A. Olive, Phys. Lett. B **508**, 65 (2001), hep-ph/0102331
54. T. Ibrahim, P. Nath, Phys. Rev. D **62**, 015004 (2000)
55. T. Moroi, Phys. Rev. D **53**, 6565 (1996); M. Carena, G.F. Giudice, C.E. Wagner, Phys. Lett. B **390**, 234 (1997); K.T. Mahanthappa, S. Oh, Phys. Rev. D **62**, 015012 (2000); T. Blazek, hep-ph/9912460; U. Chattopadhyay, D.K. Ghosh, S. Roy, Phys. Rev. D **62**, 115001 (2000)

56. A. Czarnecki, B. Krause, W.J. Marciano, Phys. Rev. D **52**, 2619 (1995), and Phys. Rev. Lett. **76**, 3267 (1996)
57. T. Falk, K.A. Olive, M. Srednicki, Phys. Lett. B **339**, 248 (1994)
58. K.A. Olive, G. Steigman, T.P. Walker, Phys. Rept. **333**, 389 (2000) [astro-ph/9905320]
59. C. Pryke et al., astro-ph/0104490; C.B. Netterfield et al., astro-ph/0104460
60. L. Ferrarese et al., astro-ph/9909134
61. J. Ellis, T. Falk, G. Ganis, K.A. Olive, Phys. Rev. D **62**, 075010 (2000)
62. J.L. Feng, K.T. Matchev, Phys. Rev. D **63**, 095003 (2001) [hep-ph/0011356]
63. J.L. Feng, T. Moroi, Phys. Rev. D **61**, 095004 (2000) [hep-ph/9907319]
64. J.L. Feng, K.T. Matchev, T. Moroi, Phys. Rev. Lett. **84**, 2322 (2000) [hep-ph/9908309]; J.L. Feng, K.T. Matchev, T. Moroi, Phys. Rev. D **61**, 075005 (2000) [hep-ph/9909334]
65. M. Brhlik, G.J. Good, G.L. Kane, Phys. Rev. D **59**, 115004 (1999) [hep-ph/9810457]
66. J. Ellis, G. Ganis, D.V. Nanopoulos, K.A. Olive, Phys. Lett. B **502**, 171 (2001) [hep-ph/0009355]
67. J.L. Feng, K.T. Matchev, F. Wilczek, Phys. Rev. D **63**, 045024 (2001) [astro-ph/0008115]
68. Physics at Run II – Supersymmetry/Higgs Workshop, Fermilab, February – November 1998, http://fnth37.fnal.gov/susy.html; M. Carena et al., hep-ph/0010338
69. H. Baer, R. Munroe, X. Tata, Phys. Rev. D **54**, 6735 (1996) [Erratum-ibid. D **56**, 4424 (1996)] [hep-ph/9606325]
70. G. Jungman, M. Kamionkowski, K. Griest, Phys. Rep. **267**, 195 (1996); http://t8web.lanl.gov/people/jungman/neut-package.html
71. N. Gray, D.J. Broadhurst, W. Grafe, K. Schilcher, Z. Phys. C **48**, 673 (1990)
72. S. Mrenna, Comput. Phys. Commun. **101**, 232 (1997) [hep-ph/9609360]
73. N. Godbane, S. Katsanevas, P. Morawitz, E. Perez, SUSYGEN 3.0, A Monte Carlo Event generator for MSSM sparticle production for lepton $(ee, \mu\mu)$, ep and hadron colliders, http://lyoinfo.in2p3.fr/susygen/susygen3.html and hep-ph/9909499
74. S. Abel et al. [SUGRA Working Group Collaboration], hep-ph/0003154
75. K.T. Matchev, D.M. Pierce, Phys. Rev. D **60**, 075004 (1999) [hep-ph/9904282]
76. H. Baer, M. Drees, F. Paige, P. Quintana, X. Tata, Phys. Rev. D **61**, 095007 (2000) [hep-ph/9906233]; V. Barger, C. Kao, Phys. Rev. D **60**, 115015 (1999) [hep-ph/9811489]; K.T. Matchev, D.M. Pierce, Phys. Lett. B **467**, 225 (1999) [hep-ph/9907505]
77. J. Nachtman, D. Saltzberg, M. Worcester [for the CDF Collaboration], hep-ex/9902010
78. H. Baer, C. Chen, M. Drees, F. Paige, X. Tata, Phys. Rev. D **58**, 075008 (1998) [hep-ph/9802441]
79. J.D. Lykken, K.T. Matchev, Phys. Rev. D **61**, 015001 (2000) [hep-ph/9903238]
80. H. Baer, C. Chen, F. Paige, X. Tata, Phys. Rev. D **54**, 5866 (1996) [hep-ph/9604406]
81. J.L. Feng, T. Moroi, Phys. Rev. D **58**, 035001 (1998) [hep-ph/9712499]
82. R. Culbertson et al., hep-ph/0008070
83. R. Demina, J.D. Lykken, K.T. Matchev, A. Nomerotski, Phys. Rev. D **62**, 035011 (2000) [hep-ph/9910275]
84. H. Baer, C. Chen, M. Drees, F. Paige, X. Tata, Phys. Rev. D **59**, 055014 (1999) [hep-ph/9809223], and references therein
85. S. Ambrosanio et al., hep-ph/0012192
86. M. Kazana, G. Wrochna, P. Zalewski, Study of the NLSP from GMSB models in the CMS detector at LHC, CMS CR 1999/019
87. TESLA Technical Design Report, DESY-01-011, Part II, The Accelerator (March 2001)
88. J. Bagger et al. [American Linear Collider Working Group], The Case for a 500-GeV e^+e^- Linear Collider, SLAC-PUB-8495, BNL-67545, FERMILAB-PUB-00-152, LBNL-46299, UCRL-ID-139524, LBL-46299, Jul 2000, hep-ex/0007022
89. T. Abe et al. [American Linear Collider Working Group Collaboration], Linear Collider Physics Resource Book for Snowmass 2001, SLAC-570, hep-ex/0106055, hep-ex/0106056, hep-ex/0106057 and hep-ex/0106058
90. S. Matsumoto et al. [JLC Group], JLC-1, KEK Report 92-16 (1992)
91. G.A. Blair, W. Porod, P.M. Zerwas, Phys. Rev. D **63**, 017703 (2001) [hep-ph/0007107]
92. G. Moortgat-Pick, H. Steiner, Physics Opportunities with Polarized e^+ and e^- Beams at TESLA, DESY-00-178, LC-TH-2000-055 (2000)
93. E. Boos et al., Nucl. Inst. Meth. A **472**, 100 (2001), hep-ph/0103090
94. S. Söldner-Rembold, G. Jikia, Nucl. Inst. Meth. A **472**, 133 (2001), hep-ex/0101056
95. R.W. Assmann et al. [CLIC Study Team], A 3-TeV e^+e^- Linear Collider Based on CLIC Technology, ed. G. Guignard, CERN 2000-08
96. CLIC Physics Study Group, http://clicphysics.web.cern.ch/CLICphysics/
97. I. Hinchliffe, F.E. Paige, Phys. Rev. D **60**, 095002 (1999) [hep-ph/9812233]; H. Baer, J.K. Mizukoshi, X. Tata, Phys. Lett. B **488**, 367 (2000) [hep-ph/0007073]
98. M. Schmaltz, W. Skiba, Phys. Rev. D **62**, 095004 (2000) [hep-ph/0004210]; M. Schmaltz, W. Skiba, Phys. Rev. D **62**, 095005 (2000) [hep-ph/0001172]
99. A. Pomarol, R. Rattazzi, JHEP **9905**, 013 (1999) [hep-ph/9903448]; Z. Chacko, M.A. Luty, I. Maksymyk, E. Ponton, JHEP **0004**, 001 (2000) [hep-ph/9905390]; E. Katz, Y. Shadmi, Y. Shirman, JHEP **9908**, 015 (1999) [hep-ph/9906296]; I. Jack, D.R. Jones, Phys. Lett. B **482**, 167 (2000) [hep-ph/0003081]; M. Carena, K. Huitu, T. Kobayashi, Nucl. Phys. B **592**, 164 (2001) [hep-ph/0003187]; B.C. Allanach, A. Dedes, JHEP [hep-ph/0003222]; I. Jack, D.R. Jones, Phys. Lett. B **491**, 151 (2000) [hep-ph/0006116]; D.E. Kaplan, G.D. Kribs, JHEP **0009**, 048 (2000) [hep-ph/0009195]
100. T. Gherghetta, G.F. Giudice, J.D. Wells, Nucl. Phys. B **559**, 27 (1999) [hep-ph/9904378]
101. M. Drees, Y.G. Kim, M.M. Nojiri, D. Toya, K. Hasuko, T. Kobayashi, Phys. Rev. D **63**, 035008 (2001) [hep-ph/0007202]